FINAL REPORT

RESEARCH AND DEVELOPMENT TO OPTIMIZE THE HYDROGEN MASER

(June 28, 1968 to June 30, 1969)

Contract NAS5-11598

Prepared by

HEWLETT **hp** *PACKARD*

Frequency and Time Division-East, Salem Road, Beverly, Massachusetts

for

NATIONAL AERONAUTICS AND SPACE ADMINISTRATION

GODDARD SPACE FLIGHT CENTER, GREENBELT, MARYLAND

July 1969

Final Report

for

Research and Development
To Optimize the Hydrogen Maser
(June 28, 1968 to June 30, 1969)

Contract NAS5-11598

Goddard Space Flight Center

Contracting Officer: J.A. Maloney
Technical Monitor: Dr. F. G. Major

Prepared by:

Frequency and Time Div. - East
HEWLETT-PACKARD COMPANY
Beverly, Mass.

Project Manager: Dr. Richard F. Lacey

for

Goddard Space Flight Center
NATIONAL AERONAUTICS & SPACE ADMINISTRATION
Greenbelt, Maryland

TABLE OF CONTENTS

LIST OF TABLES

RESEARCH AND DEVELOPMENT
TO OPTIMIZE THE HYDROGEN MASER:
FINAL REPORT

I. INTRODUCTION

From the theory of operation of the atomic hydrogen maser, it is apparent that its performance can be markedly improved by increasing the fraction of hydrogen atoms entering its storage bulb that are in the $(F=1, m=0)$ state (Reference 1). In the conventional maser design, the beam of atoms entering the storage bulb consists principally of a mixture of the desired $(F=1, m=0)$ state and the $(F=1, m=1)$ state. The latter do not contribute to the maser's oscillation, but degrade it by line-broadening spin-exchange collisions with the radiating atoms that provide the maser's output signal.

Several workers have suggested (e.g., Reference 2) that it should be possible to eliminate the unwanted state by using a somewhat more complicated beam optics design rather than the conventional one. The conventional system consists of a single hexapole magnet through which the atomic beam of hydrogen passes. Atoms in the $(F=1, m=1)$ and $(F=1, m=0)$ states are deflected toward the axis of the magnet, while the other two states are deflected outward. The length and position of the magnet are so designed that a fraction of the atoms deflected toward the axis are focussed into the storage bulb. The proposed design uses two hexapole magnets with a space between them in which the component of atomic angular momentum parallel to the applied magnetic field is rotated 180^0: atoms in the $(F=1, m=1)$ state end up in the $(F=1, m=-1)$ state and vice versa. Atoms in the other two states should end up in the same states as before. The first magnet deflects the $(F=1, m=-1)$ and $(F=0, m=0)$ states out of the beam, and the second deflects those atoms which have undergone the transition into the $(F=1, m=-1)$ state out of the beam. By these means, the atoms remaining will be in the desired $(F=1, m=0)$ state.

The object of our work is to reduce the conceptual design to an effective, practical one. Below we discuss our steps in reaching this goal, and give our conclusions on the best way to proceed in applying our results.

II. THE FIELD OF A HEXAPOLE MAGNET

In order to make accurate calculations of atomic beam optics, one must know the strength of the field in the state selection magnets. Measurements with Hall effect magnetometers are difficult to make accurately, particularly in magnets with small gap and large gradients. We have developed a technique that permits accurate evaluation of the field in a hexapole magnet.

The two components of the field in a magnet can be expressed as:

$$B_r = \sum B_n (r/r_0)^{n-1} \cos n\theta$$

$$B_\theta = -\sum B_n (r/r_0)^{n-1} \sin n\theta$$

where r_0 is the radius of the magnet. If the hexapole magnet is symmetric and the pole tips symmetric about their midplane, the only non-zero values of B_n exist for $n=3, 9, 15$ ----, when the dominant term is for $n=3$, and the higher terms are the result of deviations of the pole tips from infinite permeability and the ideal hexapolar pole tip shape:

$$(r/r_0)^3 \cos 3\theta = 1.$$

Field Measurement in a Hexapole Magnet

The magnitude of the B_n can be determined by rotating the magnet about its axis and measuring the voltage induced in a rectangular pickup loop placed so that it is bisected by the magnet axis. If the voltage is measured with a wave analyzer, the components at the various harmonics of the rotation frequency can readily be separated. If the wire is round, with diameter d, and the rotation frequency ω is low enough so that the skin depth of the wire is large compared to d, the voltage induced by each B_n is given by the expression:

$$V_n(t) = \omega B_n \cdot 2Lr_0 \cos n\omega t \left[\frac{D}{2r_0}\right]^n \left[1 + \frac{1}{4} \binom{n}{2} \left(\frac{d}{D}\right)^2 + ---\right]$$

where L is the length of the loop, D is its diameter measured between the centers of the wire, and $\binom{n}{2}$ is the binomial coefficient.

Experimentally we find that harmonics of ω other than those for which $n=3, 9$ or 15 are present, but their amplitude is down so that they represent minor perturbations of the field. The components for $n=9$ and 15 can be minimized if the tips of the pole pieces are shaped to match the theoretically ideal shape reasonably closely.

It can be important that components B_n for $n \neq 3$ be kept negligible. Calculations of their effect on the force exerted on an atom at a distance close to r_0 from the axis show the change in the force to be surprisingly large. We have built hexapole magnets in which the pole tip profile is a circle whose radius is 56% of the radius of the hexapole magnet gap (Figure 1). For such magnets we have found typically that $B_3 = 6800$ gauss, $B_9 \sim 0$, and $B_{15} < 100$ gauss. By contrast, for a magnet whose pole tips were square, $B_3 = 6200$ gauss, $B_9 = 842$ gauss, and B_{15} was negligible. One can show in this case that the magnetic gradient at r_0 varies by more than 3:1 with changes in θ.

The measured field strength, B_3, we have obtained is lower than we had originally hoped for. Measurement of the flux density across various planes in a pole piece shows that the limitation is not saturation of the iron of the pole piece, although flux densities are as high as 18,700 gauss. We believe that the limitation in our present design is the value of the coercive force of the Alnico 8B permanent magnets that produce the magnetic field, and that a magnet alloy with a greater coercive force would give a larger field at the pole tips, even though its energy product were no larger.

Saturation in the Pole Tips

The ideal hexapole pole tip has the contour $(r/r_0)^3 \cos 3\theta = 1$, where r_0 is the radius of the magnet gap. For an ideal hexapolar field,

$$|B| = B_0 (r/r_0)^2$$

where B_0 is the field strength at a pole tip. We can estimate where saturation will occur by integrating $B \cdot dS$ over the surface of a pole tip, and equating it to the integral of $B \cdot dS$ across the tip, inside the iron. Considering a unit length of pole piece, from the two equations above we can obtain

$$dS = \left[dr^2 + (r\,d\theta)^2 \right]^{1/2} = r_0 \sec^{4/3} 3\theta \, d\theta$$

$$B = B_0 \sec^{2/3} 3\theta$$

$$\int B \cdot dS = \int_0^{\theta'} B_0 r_0 \sec^2 3\theta \, d\theta = \frac{1}{3} B_0 r_0 \tan 3\theta'$$

The flux through a surface in the pole tip will be approximated by $B r \theta'$; this is the value for half a tip, from its midplane to a surface.

$$\therefore \ B = (B_0 / 3\theta') \sec^{2/3} 3\theta' \sin 3\theta'$$

Because of the secant factor, we can see that the pole pieces must saturate as $\theta \to \pi/6$ for whatever field we have at the tips. If B_0 is 7500 gauss, saturation occurs in iron at about three times that value. Expressing θ' as $\pi/6 - \delta$, and setting $B/B_0 = 3$, from the previous equation we find

$$\delta \approx \frac{1}{3} \left[\frac{2 B_0}{\pi B} \right]^{3/2} = \frac{1}{3} \left[\frac{2}{3\pi} \right]^{3/2}$$

and that the value of r at which saturation occurs is

$$r \approx r_0 \left[\frac{\pi B}{2 B_0} \right] = 2.2 r_0$$

Generally, hexapole magnet pole pieces are not made as thick as the "ideal" shape, specifically to reduce leakage flux between them and thereby reduce the effect of saturation.

To summarize, the field in a hexapole magnet is probably more complicated than is usually assumed, and sophisticated techniques should be used to determine it. It is particularly important to be able to do this in the case of a two-magnet beam optics system because the efficiency of the system will depend on matching the design of the two magnets. To design the magnet lengths, it is necessary to know their field strength.

III. TRAJECTORY CALCULATION FOR HEXAPOLE MAGNETS

The force on an atom in a magnetic field is

$$F = \mu \cdot \nabla B$$

where μ is the effective magnetic dipole moment of the atom. For an atom with a one-electron hyperfine structure,

$$\mu = \mp \frac{x + 2m/(2I + 1)}{2(1 + 4mx/(2I+1) + x^2)^{1/2}} \left(g_J + g_I \right) \mu_0 + mg_I \, \mu_0$$

$$x = \frac{\left(g_J + g_I \right) \mu_0 B}{\Delta W}$$

ΔW is the hfs splitting in the ground state, g_I is the nuclear g-factor divided by the ratio of the proton mass to the electron mass, considered positive for positive nuclear moments; I is the nuclear spin, μ_0 is the Bohr magneton, and m is the projection quantum number for the total atomic angular momentum. The upper sign applies to the magnetic sublevels for which the total angular momentum, $F = I + J$, and the lower to those for which $F = |I - J|$. For hydrogen, $x = 1.976 \times 10^{-3} B$, where the magnetic field B is in gauss. When $x >> 1$, the dipole moment for $m = 0$ states approaches a Bohr magneton, the value, for hydrogen, for states with $m = \pm 1$. Since $x = 1$ for B a little over 500 gauss, it is a useful approximation to set $\mu = \mu_0$ for all states independent of field strength. With this approximation, in a hexapole magnet, the equations of motion of an atom are particularly simple.

Straight Bore Magnets

If x and y are the transverse coordinates of displacement, and z the coordinate parallel to the beam and magnet axis,

$$\ddot{x} = \mp \frac{2\mu B_0}{mr_0^2} x$$

$$\ddot{y} = \mp \frac{2\mu B_0}{mr_0^2} y$$

where m is the mass of the atom, r_0 the radius of the magnet, and B_0 the magnetic field at the pole tips, assuming an ideal hexapolar field. The upper sign applies to the states deflected toward weaker magnetic fields, and the lower to those deflected toward stronger magnetic fields. x and y may conveniently be expressed as functions of z instead of time if we recognize that the x and y components of velocity are always small compared to the z component: $V_z \doteq V$. Then

$$\frac{d^2x}{dz^2} = \mp \frac{2\mu B_0}{mv^2 r_0^2} x$$

and similarly for y. The solutions of these equations are apparent; when the minus sign applies,

$$x = x_0 \cos(\beta z/r_0) + (x_0' r_0/\beta) \sin(\beta z/r_0)$$

where $\beta = (2\mu B_0/mv^2)^{1/2}$, x_0 is the value of x at z = 0, and x_0' is the value of dx/dz at z = 0. When the force is divergent,

$$x = x_0 \cosh(\beta z/r_0) + (x_0' r_0/\beta) \sinh(\beta z/r_0)$$

If the deflection force were not linear--i.e., directly proportional to distance from the magnet axis--the equations for x and y would no longer be independent, and general solutions in analytic form could not be obtained.

Tapered Hexapole Magnets

It has been suggested that hexapole state selection magnets with tapered bores might be advantageous in hydrogen maser beam optics systems. The trajectory of an atom with constant dipole moment can be solved analytically for this case, also. We neglect the z component of the force of the magnet, assuming the entire force is perpendicular to the axis, and assume again that $V_z \doteq V$.

Let the radius at a position z in the tapered magnet be

$$r = r_0 (1 + kz/r_0) .$$

where k is the amount of taper. The differential equation is then

$$\frac{d^2x}{dz^2} = \mp \frac{2\mu B_0}{mv^2 r_0^2} \frac{x}{(1+kz/r_0)^2}$$

The equation is simplified by making the substitution

$$u = \ln(r_0 + kz)$$

We then obtain the equation

$$\frac{d^2x}{du^2} - \frac{dx}{du} \pm \left(\frac{2\mu B_0}{mv^2 k^2}\right) x = 0$$

With the parameter $\eta = (2\mu B_0/mv^2 k^2 \mp 1/4)^{1/2}$, the solutions are

$$x = x_0 (1+kz/r_0)^{1/2} \left\{ \cos\left[\eta \ln(1+kz/r_0)\right] - (1/2\eta) \sin\left[\eta \ln(1+kz/r_0)\right] \right\}$$
$$+ x_0' (1+kz/r_0)^{1/2} (r_0/k\eta) \sin\left[\eta \ln(1+kz/r_0)\right]$$

when the upper sign applies (converging deflection) and a similar expression with the trigonometric functions replaced by the corresponding hyperbolic ones when the lower sign is appropriate (diverging deflection). Similar expressions hold for y.

These general analytic formulae are valuable when we are interested in considering the finite size of the source of hydrogen atoms. If the atoms do not start precisely on the axis of the beam optics system, we can still, by using these solutions, accurately evaluate the beam optics. There are cases when the finite diameter of the source cannot safely be neglected. We discuss how these solutions are used in the following section.

IV. MAPPING

We notice that the solutions for the atomic trajectories in the previous section are expressed in the form:

$$x(z) = x_0 \, f(z) + x_0' \, g(z)$$

where $f(z)$ and $g(z)$ are solutions of the differential equation. The slope $x' = dx/dz$ can also be expressed in a similar form:

$$x'(z) = x_0 \, f'(z) + x_0' \, g'(z)$$

The functions f and g will be different in different magnets, but the form will be the same, even in a drift region outside the magnets. In a magnet, f and g are functions of velocity. It has been shown (Reference 3) that the solutions of the differential equations for the atomic trajectories can be used as mapping transformations that facilitate the evaluation of an atomic beam optics system. If

$$x_1(z_1) = x_0 \, f_1(z_1) + x_0' \, g_1(z_1)$$

$$x_1'(z_1) = x_0 \, f_1'(z_1) + x_0' \, g_1'(z_1)$$

and

$$x_2(z_2) = x_1(z_1) \, f_2(z_2 - z_1) + x_1'(z_1) \, g_2(z_2 - z_1)$$

$$x_2'(z_2) = x_1(z_1) \, f_2'(z_2 - z_1) + x_1'(z_1) \, g_2'(z_2 - z_1)$$

we can express $x_2(z_2)$ and $x_2'(z_2)$ as linear functions of x_0 and x_0':

$$x_2(z_2) = x_0 F_2 + x_0' \, G_2$$

$$x_2'(z_2) = x_0 F_2' + x_0' \, G_2'$$

where

$$F_2 = f_1(z_1) \, f_2(z_2 - z_1) + f_1'(z_1) \, g_2(z_2 - z_1)$$

$$G_2 = g_1(z_1) f_2(z_2 - z_1) + g_1'(z_1) g_2(z_2 - z_1)$$

$$F_2' = f_1(z_1) f_2'(z_2 - z_1) + f_1'(z_1) g_2'(z_2 - z_1)$$

$$G_2' = g_1(z_1) f_2'(z_2 - z_1) + g_1'(z_1) g_2'(z_2 - z_1)$$

Similar relations hold for further steps, and may be obtained by iteration. They have the form

$$F_n = F_{n-1} f_n(z_n - z_{n-1}) + F_{n-1}' g_n(z_n - z_{n-1}) \quad \text{etc.}$$

We see that after n steps

$$x_n(z_n) = x_0 F_n + x_0' G_n$$

$$x_n'(z_n) = x_0 F_n' + x_0' G_n' \quad \text{etc.}$$

Now consider a circle in the $x - y$ plane at z_n, centered on the axis, and of radius R.

$$x_n^2 + y_n^2 = R^2$$

Substituting the values of x_n and y_n in terms of x_0 and x_0' we get

$$(x_0 F_n + x_0' G_n)^2 + (y_0 F_n + y_0' G_n)^2 = R^2$$

We can, with complete generality, choose our coordinate system so that $y_0 = 0$. Transforming this equation we have

$$(x_0' + x_0 F_n/G_n)^2 + y_0'^2 = (R/G_n)^2$$

In the "slope" space with coordinates x_0' and y_0', our circle has been trans-formed into another circle of radius R/G_n centered at $-x_0 F_n/G_n$. If the original circle of radius R represents a target aperture, such as the entrance hole of the storage bulb of a hydrogen maser, then the transformed equation represents the boundary of the solid angle at the point x_0 of the source in which atoms will be deflected into the target. We assume that the slopes are small enough so that the slope (tan θ) may be taken equal to the angle (θ). We must also, of course,

allow for collisions with other stops and apertures along the way. We can transform each circular aperture or stop back into the same "slope" plane of coordinates x_0' and y_0'. Each will be a circle, and if $x_0 \neq 0$, their centers will not in general coincide. The useful solid angle is then the portion of the intersection of the transforms of the limiting apertures not obscured by the transforms of any stops in the optical system.

By calculating $1/G_n$ and F_n/G_n for each n and velocity of interest, we can get, relatively inexpensively, a qualitative idea of the behavior of an atomic beam optical system, including the velocity range accepted, sensitivity to the finite size of the source, and requirements on stop sizes.

The mapping transformation scale factors can also be used to draw the actual maps of the overlapping circles to help the designer visualize what is going on. It must be recognized, of course, that the limited number of apertures calculated cannot completely represent the optical system; atoms will be stopped at points between them. But for some designs the approximation is very good. In the next section we discuss how we use the mapping transformations and other approximations to estimate the performance of beam optics systems.

V. CALCULATION OF PERFORMANCE OF BEAM OPTICAL SYSTEMS

We have estimated the performance of hypothetical designs of beam optical systems in two different ways. The first involves the use of the mapping transformations described above, and the second involves calculating the trajectories of atoms point by point through the system.

In the first method, using a program named MAPSIN (Appendix I), we find the area of the intersections of the circles representing the target aperture and the entrance and exit apertures of the two state-selecting magnets. This is done for a series of values of x_0 for each velocity in a series of velocities. This area represents the solid angle inside which atoms from the point x_0 of the source can reach the target aperture. Weighting each area appropriately for its origin and velocity, we sum them to find the total signal.

This area generally is irregular in shape, and we have chosen to find it by the unbiased, but computationally inefficient method of hit-or-miss Monte-Carlo, in which the components of the initial slope, dx/dz and dy/dz, are chosen randomly and tested to see if they lie within the solid angle of acceptance. The size of the solid angle is proportional to the fraction of the random initial slopes that lie within it.

It turns out that, for reasonable designs, the limiting aperture is the exit of the first magnet for the dominant part of the intensity. That is, if we plot intensity as a function of velocity, for the dominant part of the curve the useful solid angle is that defined by trajectories that graze the exit aperture of the first magnet. Here we are deceived somewhat by our calculations, because for the slower range of velocities the actual limiting aperture should be some distance within the magnet. Therefore the calculated intensities are larger than they should be. The effect can be reduced somewhat by limiting the maximum initial slope allowed to that obtained from energy considerations for an atom originating on axis within the magnets:

$$\left[\left(\frac{dx}{dz}\right)^2 + \left(\frac{dy}{dz}\right)^2 \right]^{1/2} \doteq \left[\frac{2\mu B_0}{m v^2} \right]^{1/2}$$

Since we specifically wish to consider atoms originating outside the magnet and off-axis, the above restriction improves, but does not perfect the calculation.

The second method we use to estimate the performance of a given design is the straightforward one of calculating the trajectory of the atom from point to point along its path. This problem is simplified greatly if we can assume that the atom originates on the axis of symmetry of the hexapole magnets. In that case we need consider only one dependent coordinate, i.e., the displacement of the atom from the axis. If at any point z along the atom's path we specify its displacement r and slope dr/dz, we calculate its trajectory between z and $z + \Delta z$ by assuming it is acted upon by a constant force, which we calculate for r at z, over the interval Δz. We then repeat the procedure until the atom reaches its target or runs into an obstacle. We repeat this for a series of initial slopes and a series of velocities, integrating, with appropriate weighting, over the successful initial slopes, and again over the range of velocities. The program for doing this, called STRAFO, is listed in Appendix II.

For the case of principal interest to us the results of the two methods have been reasonably consistent with each other. They can lead to markedly different results in two circumstances. The first is when the magnet next to the source is so long that atoms oscillate inside it; that is, are deflected back toward the center and cross over to the other side, to be deflected inward again. It is clear that having a limiting aperture at the exit only does not limit the possible trajectories sufficiently to approximate the actual situation where they might collide with the edge of the magnet over a considerable length. The mapping method breaks down here, although the limitation on solid angle improves the situation, of course. The second circumstance where the two methods differ is when the distance from the magnet to the target aperture is long, and the source radius not sufficiently small. We have made calculations for systems in which the second method we have described (STRAFO) gave quite favorable results, but using the first, which takes off-axis source points into consideration, the efficiency appeared to be very poor.

In Figs. 2A and 2B are shown the velocity distributions calculated with the two programs for the beam optics systems whose dimensions are given in Table I. The program STRAFO is shown twice, once with the magnet's force on the atom assumed to be proportional to displacement from the axis, and again when the force is derived from the Breit-Rabi expression for states with $m = 0$. The limitation in the program MAPSIN is the limitation on initial slope mentioned above that rejects some trajectories which would otherwise hit the pole pieces of the first magnet. The integrated areas of the curves in Figs. 2A and 2B are given in Table II.

The area under these curves represents the fraction of atoms in the $(F = 1, m = 0)$ state effused from the source collimator of the hydrogen maser that reach the target aperture. We assume that the collimator consists of round tubes whose length is ten times their diameter, and we neglect the dependence of intensity with angle for the entire angle of acceptance. For the design velocity, the maximum initial angle transmitted is $\theta_{max} = \sqrt{2\mu B_0 / 3kT}$, equal to approximately .03 rad for 7500 gauss magnets. The characteristic width of the angular distribution, the ratio of collimator diameter to length, is 0.1. While θ_{max} is not very small compared to .1, neglecting the variation of intensity is a reasonable approximation that greatly simplifies computation (Reference 5). We also assume that the effused hydrogen atoms have a Maxwell-Boltzmann distribution with a characteristic temperature of 380^0K.

The dimensions of the system labeled "space maser" are those of an actual experimental maser. Those labeled "double magnet" refer to a proposed design that we believe to be most practical for our state filter beam optics system. Notice that their efficiencies are comparable. The double magnet system, as computed, is more efficient than designs that have successfully been used. For example, with a system whose dimensions are identical with the space maser, except that the distance from the magnet to the target aperture is 30 inches, the fractional intensity, assuming the Breit-Rabi exact force law, is 1.5×10^{-3}. This is markedly less than the 2.87×10^{-3} calculated for the double magnet system (Table II). In all these calculations we have not included any stops. Taking them into account would reduce the intensity a little, and clip

Table I -- Beam Optics System Dimensions

(Linear Dimensions in Inches)

	Space Maser	Double Magnet
Collimator to First Magnet	.125	.125
First Magnet Length	3.0	2.112
First Magnet Diameter	.125	.080
First-to-Second Magnet	--	4.0
Second Magnet Length	--	7.0408
Second Magnet Diameter	--	.125
Second Magnet to Target	9.0	10.0
Target Diameter	.226	.226
Maximum Magnet Field Strength	7500G	7500G
Source Collimator Diameter	.020	.010

Table II -- Fractional Efficiency

	Space Maser	Double Magnet
MAPSIN with limitation	4.92×10^{-3}	3.66×10^{-3}
STRAFO with linear force law	4.56×10^{-3}	3.15×10^{-3}
STRAFO with Breit-Rabi force law	4.33×10^{-3}	2.87×10^{-3}

the high velocity tail of the curves. The differences between the three computed values are small, we feel, as beam optics computations go, and we will not be misled in using them.

In choosing our design for the two magnet system, we had to consider not only efficiency for the case illustrated where both magnets deflect the atoms toward their axis, but also those cases where one magnet deflects inward and the other outward. For the state filter system to work, the transmission in such cases must be negligible compared to the desired case. The system we found that does this best is shown schematically in Figure 3, and its dimensions are given in Table I (double magnet).

The dimensions were arrived at in the following way. The distance between magnets, and the distance from the second magnet to the aperture were chosen to be short, yet still long enough so that magnetic shielding problems would not be inordinately difficult either in the transition region between the magnets nor in the storage bulb. The diameter of the second magnet gap was chosen to be .125 inch because that is the diameter that has been most used. The diameter of the first magnet gap was chosen to be .080 inch, to be smaller than the second, but still practicable to build. We assumed a peak magnetic field strength of 7500 gauss, and chose the length of the first magnet so that an atom with the most probable velocity of the velocity distribution ($1.22\,\alpha$) will leave the magnet parallel to the axis if it originates at the axis at the entrance to the magnet. That is,

$$x' = x_0' \cos(\omega \ell/r_0) = 0$$

where $\omega = (2\mu B_0/3kT)^{1/2}$. This condition holds when the argument of the cosine is $\pi/2$, or $\ell = \pi r_0/2\,\omega$. The criterion for the length of the second magnet is that trajectories of atoms with the modal velocity parallel to the axis pass through the center of the target aperture. That is, at the exit of the second magnet

$$\frac{dx}{dz} = -\frac{x}{L}$$

where L is the distance from the magnet to the aperture.

$$x = x_0 \cos \omega \ell / r_0$$

$$\frac{dx}{dz} = -(x_0 \omega / r_0) \sin \omega \ell / r_0$$

$$\therefore \cot (\omega \ell / r_0) = \omega L / r_0$$

The first solution of this transcendental equation results in a very short magnet, which will not reject unwanted states very well, so we use the second, which gives us the trajectory shown in the middle diagram of Figure 3. This mode of trajectory is successful for a range of velocities about the design velocity. A substantial contribution to the useful flux at the target aperture is made by slower atoms whose typical trajectory is shown in the bottom diagram. The two velocity ranges are marked by the cleft in one of the intensity curves in Fig. 2B. With the other two, the two velocity intervals overlap. By varying the magnet lengths 10% about those given in Table I, we showed that these dimensions, designed to focus the most probable velocity, were optimum. The fractional intensity reaching the target aperture was 2.87×10^{-3} for the optimum design (calculated using the program STRAFO); and 2.68×10^{-3} if the magnets were 10% shorter, and 2.79×10^{-3} if they were 10% longer.

Tapered First Magnet

In Figure 4 we show the intensity distribution curves for the case where the first magnet is tapered slightly. The initial diameter is .080 inch, and the taper is .0034. The length of the magnet is increased to 2.4 inches to match the criterion by which we determined the length of the straight bore magnet. The total intensity in each case is about 10% greater than for the corresponding calculation with a straight bore magnet. We deem the improvement too slight to justify the use of a tapered magnet in view of the difficulty in accurately measuring its magnetic field.

VI. ADIABATIC FAST PASSAGE AND RABI RESONANCE

Adiabatic fast passage is a method well known in nuclear magnetic resonance for reversing the orientation of a spin system, particularly useful when the resonance is broadened by magnetic field inhomogeneity. It is also useful in molecular beams to reverse the direction of spin (i.e., change the sign of the magnetic quantum number m) in a beam with a broad velocity distribution. We are concerned with the molecular beam case, in which the polarized beam traverses a region in which there is a magnetic field with a weak gradient. The beam travels in the direction of the gradient and at right angles to the field. An oscillating magnetic field whose frequency matches that required to induce the spin flip transition at the midpoint of the static field is applied over an extended region. The magnetic gradient causes the atomic resonance frequency to vary about that of the oscillating field as the atoms pass through. If the change in value of the static field that the atom sees is slow enough, and the oscillating field is strong enough, the direction of the spins will be rotated by 180^0, independent of velocity.

We may contrast this with the more usual sort of transition, which we will refer to as a Rabi transition, induced in a region where the static field is homogeneous. The oscillating field strength will be much lower than in the former case, and whether the spin is rotated by 180^0 or by more or less will depend on the strength of the oscillating field and the length of time it acts on the atom.

If the velocity distribution is narrow, there may not be much practical difference between using either method to produce the 180^0 rotation we need for our state filter beam optics system. It would be a matter of convenience.

It is quite simple to calculate the effect of the oscillating field for particles of spin $\frac{1}{2}$ for either the adiabatic fast passage case or the Rabi case. We need to calculate the transition probability for going from the state $m = \frac{1}{2}$ to the state $m = -\frac{1}{2}$. The comparable transition probabilities when the angular momentum is greater than $\frac{1}{2}$ can be obtained from the well known

formula of Majorana (Reference 4, pp. 427-430). We are interested, for hydrogen, in the $F=1$ level, where the total angular momentum is 1. If we call the probability for the $(m=\frac{1}{2}, m=-\frac{1}{2})$ transition of a spin $\frac{1}{2}$ particle T, then the Majorana formula gives the following results for $T_{m,m'}$, the probability that a particle in state m initially ends up in state m'.

$$T_{1,1} = (1-T)^2 \qquad\qquad T_{0,1} = 2T(1-T)$$
$$T_{1,0} = 2T(1-T) \qquad\qquad T_{0,0} = (1-2T)^2$$
$$T_{1,-1} = T^2 \qquad\qquad\qquad T_{0,-1} = 2T(1-T)$$
$$(0 \le T_{m,m'} \le 1)$$

Hydrogen maser optics will, in the absence of induced transitions in the beam, focus atoms in the $(F=1, m=1)$ and $(F=1, m=0)$ states into the storage bulb with approximately equal probability. Using the two-magnet system described above, where the first magnet deflects out atoms in the $(F=1, m=-1)$ and $(F=0, m=0)$ states from the beam, a reversal of spin direction is induced and the second magnet deflects out atoms now in the $(F=1, m=-1)$ state, the ratio of intensity of atoms in the $(F=1, m=0)$ state to the total intensity focussed into the storage bulb is given by

$$\frac{I_{m=0}}{I_{tot}} = \frac{1 - 2\epsilon + 2\epsilon^2}{1 + \epsilon^2}$$

where $\epsilon = 1-T$. For small values of ϵ this ratio is approximately $1-2\epsilon$. The expression is shown graphically in Figure 5. For values of ϵ between .33 and 1, (or T between 0 and .67), the ratio is less, and the performance of the maser worse, than if no transitions at all were induced.

Calculating T: For a Rabi type of induced transition, in which the atom's resonance frequency is constant over the region where the oscillating field inducing the transition is applied, the transition probability T is given by the expression (Reference 4, pp. 146-151):

$$T = \frac{(2b)^2}{\beta^2 + (2b)^2} \sin^2 \frac{1}{2}\left[\Omega^2 + (2b)^2\right]^{1/2} t$$

where   b = matrix element of interaction inducing the transition,

Ω = $\omega_r - \omega$, the resonance frequency minus the applied frequency,

t = length of time the interaction is applied to atom.

We assume that b is constant over the interval t, and that the oscillating field is decomposed into two rotating components, one of which is ignorable. At resonance ($\Omega = 0$) this function is a maximum, evidently, for sin bt = 1, or bt = $\pi/2$.

In adiabatic fast passage, the value of Ω changes continuously. We calculate the transition probability by dividing up the interval of time during which the atom passes through the interaction region into many small intervals, assuming that b is the same in all of them, and that Ω is constant in each, changing discontinuously from one interval to the next. We describe this calculation in detail in Appendix III. The principle of adiabatic fast passage can be visualized with the help of Figure 6. The energy difference between the states is shown as μH_z, or the equivalent frequency $\mu H_z / \hbar$. The effect of being in a rotating coordinate system, in essence subtracting away some of the Larmor precession, is represented by the vector ω in the opposite (-z) direction. The contribution due to the rotating component of the field inducing the transitions is shown by the vector lying on the x axis in the rotating coordinate system. The resolvent vector sum of these three will move from being nearly parallel to the +z axis to being nearly parallel to the -z axis as H_z slowly decreases. The resolvent vector is equivalent to an effective magnetic field, and if the change is slow enough, an atom originally aligned parallel to the z axis will follow the resolvent vector adiabatically, reversing its spin direction.

The transition probability as a function of rate of passage is shown in comparison with that for a Rabi type of induced transition in Figure 7. The relation between the abscissas of the two curves is arbitrary. The maximum of the Rabi curve occurs when bt = $\pi/2$ radians. The quantity b must be bigger in the adiabatic fast passage technique, and we have made the point where bt = 10 radians coincide with the maximum of the Rabi curve. The

quantity t is the time of flight through the entire coil in both cases. Schematic diagrams of the apparatus in which the two types of transition might be induced are shown in Figure 8, with the Rabi resonance region shown as A, and the adiabatic fast passage region shown as B.

As it turns out, for $\Delta t/t \leq .4$, which is about the spread in times of flight we expect from our beam optics calculations, and assuming optimum tuning, it makes no significant difference which method of rotating the atomic spins we use. The efficiency of the two methods is practically identical, and our choice must be indicated by other considerations.

To design the adiabatic fast passage apparatus we must first choose a value of bt large enough so that the transition probability is close to 1 for the whole velocity range of interest. We must also choose the length of the coil, the fractional gradient $\Delta H/H$ over the length of the coil, and how far the resonance frequency of the atom is from the applied frequency when the atom enters and leaves the coil. (It should be at resonance in the middle.) For example, let us choose as follows:

$$bt \geq 15 \text{ radians}$$
$$\Omega_{initial} = 10b$$
$$\Delta H/H = .1$$
$$\ell = 5 \text{ cm.}$$

Then $2\pi\mu\,\Delta H = 20b$, where $\mu = 1.4 \times 10^6$ Hz/G.

$$\Delta H/H = 20b/2\pi\mu H = .1$$

$$\therefore H = 200b/2\pi\mu$$

$$\text{and } \mu H = 100b/\pi$$

The mean velocity V in a hydrogen beam will be $\approx 3 \times 10^5$ cm/sec.

$$bt = b\ell/V \geq 15$$

$$\therefore b \geq 15V/\ell = 9 \times 10^5$$

$$\text{and } \mu H \geq 9 \times 10^7/\pi = 28.6 \text{ MHz}$$

$$H \geq 20.4 \text{ gauss}$$

This gives the minimum frequency we should apply to the coil and the corresponding magnetic field at its middle. We can obtain the strength of the oscillating field required from the relation for a spin $\frac{1}{2}$ particle whose g factor equals that of a hydrogen atom:

$$\hbar b = 2\pi\mu g_J < J = \tfrac{1}{2}, \; m = \tfrac{1}{2} \; |J_x| \; J = \tfrac{1}{2}, \; m = -\tfrac{1}{2} > \; \cdot \; \tfrac{1}{2} H_{osc}$$

In this case $g_J = 1$, and the matrix element equals $\frac{1}{2} \hbar$.

$$\therefore \; H_{osc} = 2b/\pi\mu$$

$$H_{osc} \geq 2 \times 9 \times 10^5 / \pi \times 1.4 \times 10^6 = .408 \text{ gauss.}$$

The factor of $\frac{1}{2}$ multiplying H_{osc} is required because the spin interacts with a rotating component of H_{osc} rather than with the entire oscillating field.

In the case of a Rabi resonance, the design is simpler, and the strength of the oscillating field has no relation to the strength of the static field. One would probably choose to design the region where the transition is induced to be similar to the C field of a cesium beam tube, as is shown in Figure 8 That is, there would be a magnetically shielded region in which a relatively weak, uniform, static magnetic field is maintained. The length of the coil can be quite short, the frequency lower ($\approx 10^6$ Hz), and the strength of the oscillating field somewhat less. It is necessary for $\omega t / 2\pi > 1$, so that atoms cannot pass through the coil while the oscillating field is close to zero.

$$bt = \pi/2 = b\ell/V$$

If $\ell = 1$ cm

and $V = 3 \times 10^5$ cm/sec.,

then $b = 4.71 \times 10^5$

and $H_{osc} = 2b/\pi\mu = .204$

Relative Merits of Adiabatic Fast Passage and Rabi Resonance Transition Methods

As we stated above, the choice between the two methods of rotating the spin of the atoms in the hydrogen beam must be made on grounds other than their relative effectiveness, since for the velocity distribution we expect there will be little difference between them.

The principal advantage of the Rabi method is that the design of the magnetic shielding and the uniform magnetic field utilize techniques that are well known to us. The frequency and strength of the oscillating field can be lower, too, than the other method requires. The principal disadvantage is that care must be taken to avoid Majorana transitions in going from the strong field of the hexapole magnets to the weak one when the transition is induced. (Majorana transitions in a molecular beam are induced by sudden changes in direction of the static magnetic field along its trajectory.) Another disadvantage is that the adjustment of the frequency and intensity of the oscillating field must be more precise than is required with adiabatic fast passage.

Conversely, using adiabatic fast passage, the requirements on tuning and power level are not quite as sharp, the transition from strong field to weak field should be easier, but on the other hand it represents an untried technology.

We noted above that in the Rabi method there is a requirement that $\omega t/2\pi \gg 1$ to ensure that atoms don't pass through the transition region while the oscillating field is crossing through zero. We decompose the oscillating field into two contra-rotating components, one of which can be ignored, of constant amplitude, to calculate the transition probability shown in Figure 7. This decomposition is not valid if the atom does not experience several cycles. We make the same approximation with adiabatic fast passage, but it is not clear in that case what the criterion is for the validity of the approximation.

It is our opinion, weighing all these factors, that both methods should be tried, with priority given to the adiabatic fast passage method. This should receive the emphasis both because of its advantage in looser requirements on level and frequency of the oscillating field and because it represents an advance in technique that should be tried.

VII. IMPROVEMENT OF MASER OPERATION

If quenching due to magnetic inhomogeneity over the volume of the
storage bulb of a hydrogen maser can be neglected, the mechanisms that con-
tribute to the hydrogen resonance linewidth are spin exchange collisions,
escape of atoms from the storage bulb, and loss of atoms due to recombination
on the wall of the storage bulb. Experimentally, the last two terms cannot be
distinguished, and we lump their effects on the linewidth together. We have

$$\Delta \nu = \Delta \nu_{min} + \Delta \nu_{s.e.}$$

where $\Delta \nu$ is the hydrogen resonance linewidth, $\Delta \nu_{min}$ is the portion of the line-
width due to escape from the storage bulb and recombination--i.e., the linewidth
limit as the density of hydrogen atoms approaches zero. $\Delta \nu_{s.e.}$ is the portion
of the linewidth due to spin exchange collisions between hydrogen atoms and is
proportional to atomic hydrogen density in the storage bulb, or to the total flux
of atoms entering the storage bulb:

$$\Delta \nu_{s.e.} = \frac{\sigma \bar{v} I_{tot}}{2 \pi V_b \gamma} = \Delta \nu - \Delta \nu_{min}$$

where σ = spin exchange collision cross section,

$\bar{v}$ = mean relative velocity between hydrogen atoms,

V_b = volume of the storage bulb,

γ = reciprocal of mean lifetime of hydrogen atoms in storage bulb,

I_{tot} = total flux into the storage bulb.

The total power radiated by the atoms in the storage bulb in the absence
of magnetic quenching can be expressed as:

$$P = \frac{1}{2} h \nu \left[I - \frac{h V_c}{8 \mu_0^2 \eta Q} \Delta \nu (2 \Delta \nu - \Delta \nu_{min}) \right]$$

where   I = net useful flux,

V_c = volume of the cavity,

μ_0 = Bohr magneton,

η = "filling factor" (reference 1)

Q = Planck's constant,

ν = radiated frequency.

- 23 -

The width of the hydrogen resonance line is found by measuring the shift in the radiated frequency as the cavity is detuned:

$$\nu - \nu_0 = \Delta \nu Q / \nu_0$$

where ν_0 is the exact resonance frequency, as modified by the wall shift, second-order Doppler effect, and magnetic field correction. $\Delta \nu_{min}$ can be obtained by extrapolation of the linewidth as a function of flux to zero flux.

Reducing the linewidth $\Delta \nu$ while maintaining I will obviously result in a marked increase in power output. In addition, reducing the linewidth lowers the value of flux required for the maser to oscillate at all (P > 0). Finally, the theoretical limit to the frequency stability of a maser depends on linewidth and power:

$$\sigma_f / \nu = (\Delta \nu / \sqrt{2} \, \nu) \, (kT/Pt)^{1/2}$$

where σ_f is the rms deviation in output frequency,

   k   is Boltzmann's constant,

   T   is the absolute temperature,

   t   is the averaging time interval.

As a practical matter, however, this limit is never reached because the instability due to additive noise in the external circuitry that receives the maser's signal, and long term drifts due to temperature fluctuations and the like, drown it out.

The power delivered by the maser beam is usually expressed in terms of a parameter q (Reference 1):

$$q = \frac{\sigma \bar{v}_{rel} \, \hbar}{8 \pi \mu_0^2 Q} \frac{V_c}{\eta V_b} \frac{I_{tot}}{I} .$$

q can be expressed in terms of the linewidth also, making use of the expressions given above. It is difficult to measure power or flux absolutely, but the value of I for which the power is zero can be found in terms of the linewidth by extrapolating the curve of power as a function of linewidth to zero power, $\Delta \nu'$. When P = 0 we have

$$I = \frac{hV_c}{8 \mu_0^2 \eta Q} \Delta \nu' (2 \Delta \nu' - \Delta \nu_{min}) .$$

If we assume that the ratio I_{tot}/I is a constant for all flux levels, then

$$q = \frac{\Delta \nu_{min}(\Delta \nu' - \Delta \nu_{min})}{\Delta \nu'(2\Delta \nu' - \Delta \nu_{min})}$$

The smaller the value of q, the better the performance of the maser. Note that the value of q can be obtained experimentally independent of any knowledge of cavity Q, coupling coefficient, filling factor, collision cross section, or cavity and bulb volume.

To measure the effectiveness of using adiabatic fast passage, the ratio of the values of q without and with it can be made. This will give the improvement in the ratio of the useful flux I to the total flux, I_{tot}. Ideally, the ratio of the two values of q should be 2:1.

VIII. DESCRIPTION OF APPARATUS

The experimental apparatus we built differs from the ideal design described in Table I in several respects, as shown in Table III. The first magnet was made with a .125-inch gap diameter to facilitate both measurement of its field strength and its manufacture. The second magnet was longer than desirable to make use of parts of an already existing magnet. The Alnico drivers of the two magnets came from two different lots, which may account for the difference in the measured fields. This difference in field strength meant that the lengths of the two magnets were not quite matched, since it was, of course, necessary to choose their lengths before building and measuring them. In order to make use of available existing apparatus, the source diameter was greater than would have been desirable, and the distance from the second magnet to the storage bulb aperture was twice as long as it need have been. The velocity distribution of the beam flux calculated with the parameters we actually had is shown in Figures 9, 10 and 11, and the total flux is shown in Table IV.

The maser on which the experiment was performed had a spherical storage bulb with an eighth-inch diameter. The usual storage bulb has a seven-inch diameter, and the effect of the larger size is to decrease wall effects somewhat and to make the so-called "filling factor" (References 1 and 6) smaller. The small filling factor results in the maser's having a lower output of power, while the lower rate of wall recombination results in its linewidth being narrower than is the case with masers that have a seven-inch-diameter storage bulb. Before it was modified, the maser we used had conventional beam optics and it barely oscillated. From its calculated parameters it should have oscillated reasonably well, and we can only speculate as to why it did not. Among the possibilities are misalignment, or transitions induced by magnetic gradients, either of which might introduce a background of unpolarized atoms into the storage bulb. As we shall discuss later, after the modification the maser oscillated much better.

Table III -- Comparison of Actual vs. Design Ideal, Double Magnet Systems

	Actual	Ideal
First Magnet Length	3.73	2.112
First-to-Second Magnet Distance	4.0	4.0
Second Magnet Length	7.75	7.041
Second Magnet to Storage Bulb Aperture	20	10
Source Diameter	.030	.010
First Magnet Diameter	.125	.080
Second Magnet Diameter	.125	.125
Bulb Aperture Diameter	.150	.226
First Magnet Field	7040	5400
Second Magnet Field	6500	7500
Stop Diameter	.032	0

Table IV -- Comparison of Computations of Actual Double Magnet System

Computation	Fractional Intensity
MAPSIN	4×10^{-4}
STRAFO with Breit-Rabi force	8.4×10^{-4}
STRAFO with linear force law	7.4×10^{-4}

The adiabatic fast passage region was a tapered electromagnet operated at about 20 gauss. The pole pieces were 3.25 inches long, 1 inch wide, and separated by .385 inch at their middle. They were made so that the gap between them had a uniform taper, varying a little over 8% in a distance of two inches. The pole pieces were made of Armco iron that was annealled after machining by being passed through a hydrogen atmosphere brazing furnace. The return yoke was an Armco iron cylinder one inch long and 3.5 inches O.D. mounted co-axial to the beam and state selection magnets. Two arms along one diameter supported the pole pieces, and were wound with four turns each of Teflon insulated wire. The desired 20 gauss field required 16 ampere-turns, or two amperes through the eight turns. Since there was some remanence in the magnet, another eight turns were provided through which an alternating current could be passed to eliminate the effects of remanence. Measurements of the field in the gap showed it to be uniform over the diameter of the beam, and to vary linearly with distance along the beam in the region of the coil. The change of strength of the field was in agreement with the change in gap because of the mechanical taper:

$$H \cdot d \doteq n_i$$

That is, the strength of the field times the gap width d at that point was equal to the number of ampere-turns in the magnet, as it should. The hexapole magnets adjacent to each end of the tapered magnet caused variations in the field, depending on their relative orientation, but these did not extend to the region in which the coil was mounted.

The coil, two inches long, was made of 55 turns of #21 magnet wire wound on a $^3/_{16}$-inch mandrel. Its inductance was about 1.6 μhenry. In order to drive it at 28 MHz with the signal generator available, it was necessary to resonate it with a variable capacitor mounted external to the vacuum system.

The maser used had a loaded cavity Q of 32,000 and the coupling co-efficient was 0.2. The cavity could be fine-tuned by means of a mechanical plunger operated by a screw from outside the vacuum. Unfortunately, it was not

possible to tune the cavity to the hydrogen resonance frequency, but this made no real difference to the experiment.

The two magnets and the tapered magnet were held in alignment by a rigid framework. The axis of the two magnets was aligned by eye to pass through the storage bulb aperture by adjusting the mounting of the framework. The position of the source collimator likewise was adjusted by eye to coincide with the axis. The alignment turned out to be completely adequate.

IX. EXPERIMENTAL RESULTS

The first significant experimental result is that the maser oscillated very well with its rather complicated beam optics system, both with and without the enhancement from the induced adiabatic fast passage resonance to eliminate atoms in the (F = 1, m = 1) state. The oscillation was stronger, and occurred at lower source pressures than had been the case before the modification of the beam optics, when it had been found very difficult to get the maser to oscillate at all.

In our experiments the data that could be accurately measured were the relative power from the maser and the frequency of its signal. The frequency was measured by comparison to another maser. The reference maser was used to phase-lock a 5 MHz crystal oscillator whose signal was compared, after multiplication and synthesis to a frequency close to that of the maser under study, to the frequency of the maser signal. The synthesizer was set so that the period of the beat was about 8 seconds, and the duration of 10 periods was measured with an electronic counter. For a given set of conditions (flux level, and with or without adiabatic fast passage enhancement), the beat period was recorded for each of a series of settings of the mechanical tuner. After some manipulation of the data, the slope of the curve of change of maser frequency as a function of cavity frequency offset was obtained by a least squares fit to a straight line. Also, for a given cavity frequency setting, the relative power was measured by adjusting a calibrated attenuator to bring the signal to a predetermined level. The results of a series of measurements are shown in Figure 12. In the upper section, relative flux, assumed proportional to source pressure, is plotted as a function of cavity pulling, the slope of the maser frequency versus cavity frequency curve. In the lower section the relative power is plotted against cavity pulling. The error bars represent the 2σ confidence limits on the slope deduced from the least squares regression. In each section the curve on the left, representing less pulling and hence the narrower hydrogen resonance linewidth, is the result when adiabatic fast passage transitions are being induced.

When these curves are extrapolated to zero power or zero beam intensity, we can deduce the limiting linewidths $\Delta \nu'$ and $\Delta \nu_{min}$ from the intercepts. Then, as described in Section VI, we can find the degree of enhancement; that is, the ratio of the ratios of useful flux to total flux with and without the adiabatic fast passage transition being induced.

Qualitatively, with adiabatic fast passage transitions being induced, there is a slight increase in maser power. The transient behavior, on applying the radio frequency power to the coil, is for the power to decrease for a few seconds and build up. Conversely, when the r.f. power is turned off, the power increases briefly and then declines. This is an indication that the total useful flux reaching the storage bulb of the maser is smaller when the adiabatic fast passage transition is being induced, as well as the total flux.

We find that turning on the adiabatic fast passage transition increased the power put out by the maser by about 2 db. By calculating the values of q with and without enhancement, and taking their ratio, as described above, the improvement in the ratio of useful flux to total flux was found to be approximately 20 per cent.

The degree of improvement is smaller than expected. There are several possible explanations for this. One is that Majorana transitions are occurring between the state selection magnets and the storage bulb aperture, scrambling the state populations. Originally the hydrogen beam passed through a fairly small hole ($\frac{1}{2}$ inch) in a mumetal septum, and we thought that transitions might be occurring there. However, when this hole was enlarged to two inches there was no improvement discernible. When a coil of wire was placed around the region through which the beam passed and direct current was made to flow through it, it was possible to make the performance of the maser worse for current flow in one direction, but not to improve it. It is still possible that such transitions occur somewhere else. Certainly the power level and residual linewidths are sensitive to the bias field at which the maser is operated, and to the settings of current in the coils used to trim that field.

Another reason why the improvement may not be as good as expected
is that the beam optics preferentially focus atoms in the (1, 0) state into the
storage bulb anyway. As shown in Table IV, the calculations based on the
approximation of a point source of atoms show that the (1,0) state is focussed
13% more efficiently than the (1,1) state, and the advantage might be even
greater in actuality. There may also be a background of unpolarized atoms
that finds its way into the storage bulb.

The adiabatic fast passage transition seems to work as intended. If
the power applied to the coil is too low, maser operation is quenched, but the
performance of the maser seems to be independent of power level of frequency
over a remarkably broad range, as long as the frequency corresponds to reso-
nance for the transition between the ($F = 1$) hydrogen levels near the center of
the coil.

Audoin et al (Reference 7) have operated a hydrogen maser with
similar optics and have measured the actual state population in the storage
bulb at very low flux levels in an experiment which we did not have the equip-
ment (or the time) to duplicate. They found, with adiabatic fast passage enhance-
ment, that approximately 85% of the atoms were in the desired (1,0) state. The
improvement in power of the maser in oscillation, however, was also about 2 db.

X. CONCLUSION

We have made thorough calculations that show that a hydrogen atomic beam optics system can be made that substantially focusses only atoms in the (F=1, m=0) state into the storage bulb of a hydrogen maser. The efficiency of this state filter system can be comparable to the simpler state selection systems that have generally been used. We have calculated the performance on the basis of two different approximations, and found them to agree closely for our proposed design.

We have found that it is feasible to use either a conventional Rabi resonance or an adiabatic fast passage transition to induce a 180° rotation of spin alignment in the region between the two hexapole magnets of our proposed beam optics system. We suggest that both methods be tried, with the adiabatic fast passage method given first priority.

Calculations of the effect of tapering the state selecting magnets show that flaring the first magnet results in a slight improvement in the efficiency with which hydrogen atoms from the source are used. The calculated improvement is small enough that it does not justify using a tapered magnet when the difficulties in assessing the field strength in a tapered magnet are considered.

The experimental test of the improved beam optics system showed that a relatively complicated atomic beam optics design can be made to work efficiently. The improvement obtained by using adiabatic fast passage, while not as great as expected, is useful to the operation of the maser, and there are no drawbacks to its use apart from the greater elaborateness of the design. The application of the principle to atomic hydrogen masers is practical and valuable.

XI. NEW TECHNOLOGY

The following items of new technology have developed during the work on this contract:

a) Method of analyzing the field of a hexapole magnet.

b) Design of a state selecting hydrogen beam optics system.

References

1. D. Kleppner et al., "Hydrogen Maser Principles and Techniques," Phys. Rev. 138 pp. A792-A983 (1965).

2. J.-P. Schermann, "Double focalisation dans un maser à hydrogène," Comptes Rendues 266 pp. 295-298 (1966).

3. R.T. Daly, TRG, Inc., "Study Leading to the Design of Missile-Air- and Submarine-Borne Atomic Frequency Standard," Second Quarterly Progress Report, Signal Corps Contract No. DA36-039 SC 73283, A.D. No. 201291 (1958).

4. N.F. Ramsey, Molecular Beams, Oxford University Press (1956).

5. B.B. Dayton, "Gas Flow Patterns at Entrance and Exit of Cylindrical Tubes," American Vacuum Society, Transactions of the Vacuum Symposium, 1956. Edited by Perry and Durant, Pergamon Press.

6. D. Kleppner, H.M. Goldenberg and N.F. Ramsey, "Theory of the Hydrogen Maser," Phys. Rev. 126, pp. 603-615.

7. C. Audoin, M. Desaintfuscien, P. Piejns, J.-P. Schermann, "A New Method for Measurement of the Population Difference of Hyperfine-Levels of Stored Atoms," Proc. of the 23rd Annual Frequency Control Symposium, Atlantic City, N.J., May 6-8, 1969.

ARMCO IRON

ALNICO - 8B

DETAIL
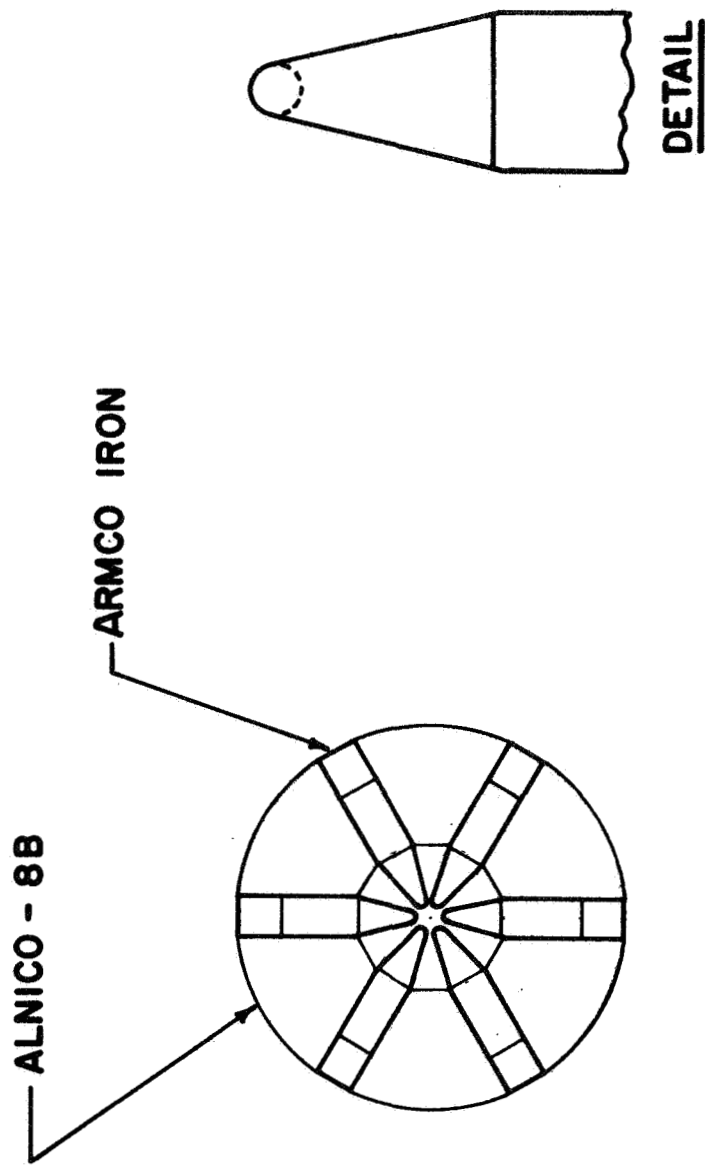
HEXAPOLE MAGNET

Figure 1.

SPACE MASER

MAPSIN W/ RESTRICTION

STRAFO W/ LINEAR FORCE

STRAFO W/ BREIT-RABI

V/α

2
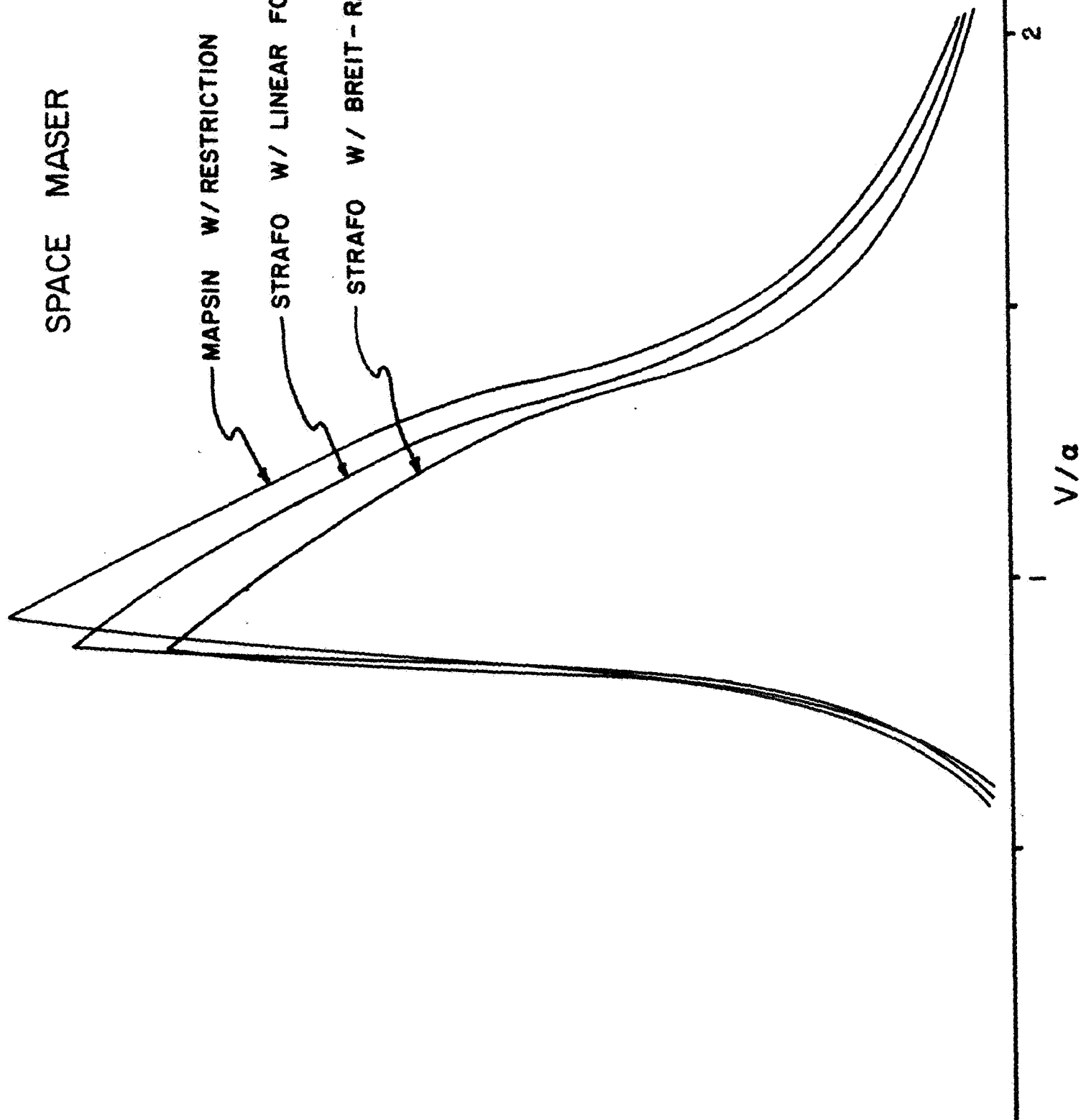
Figure 2A

TWO MAGNET SYSTEM
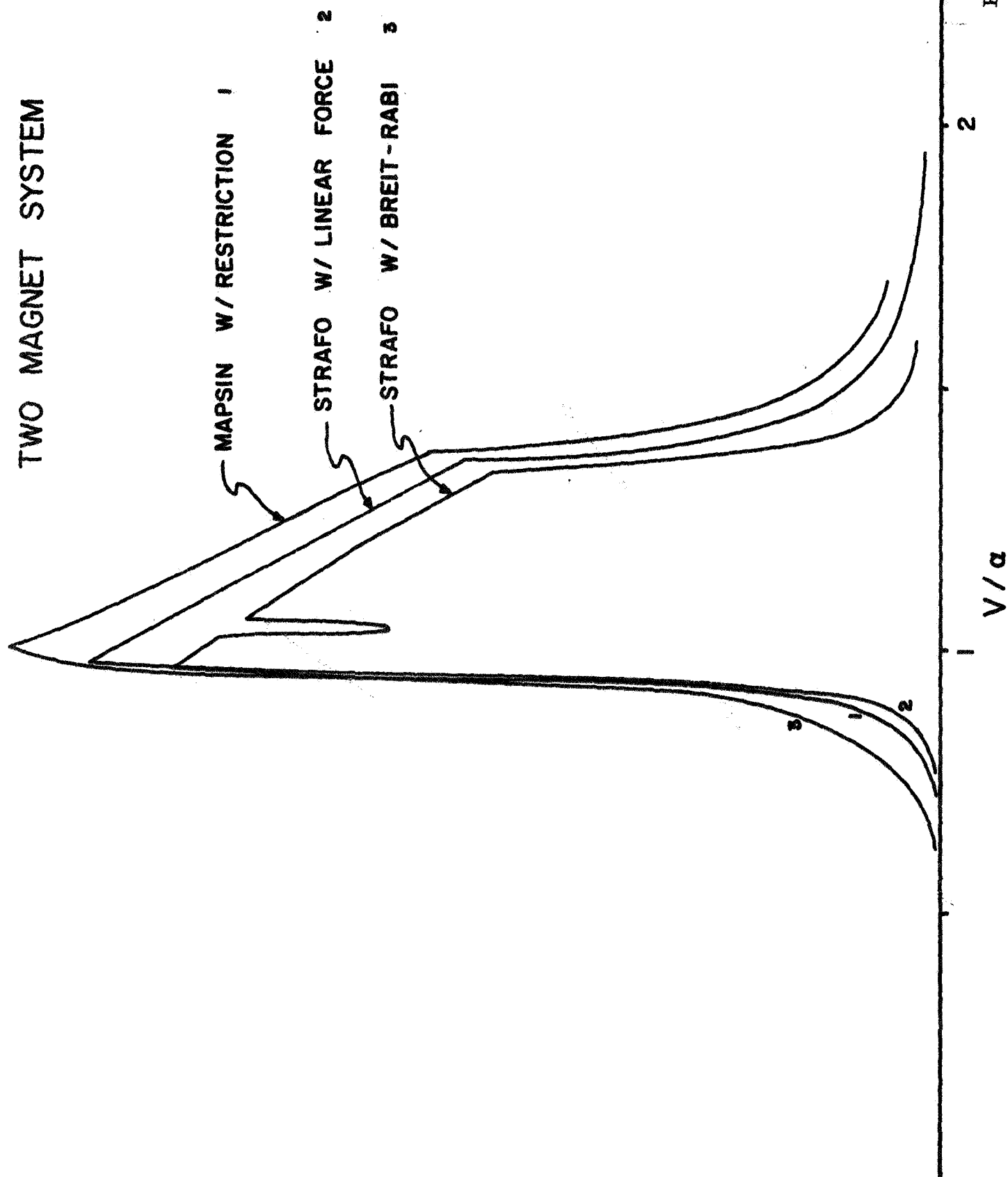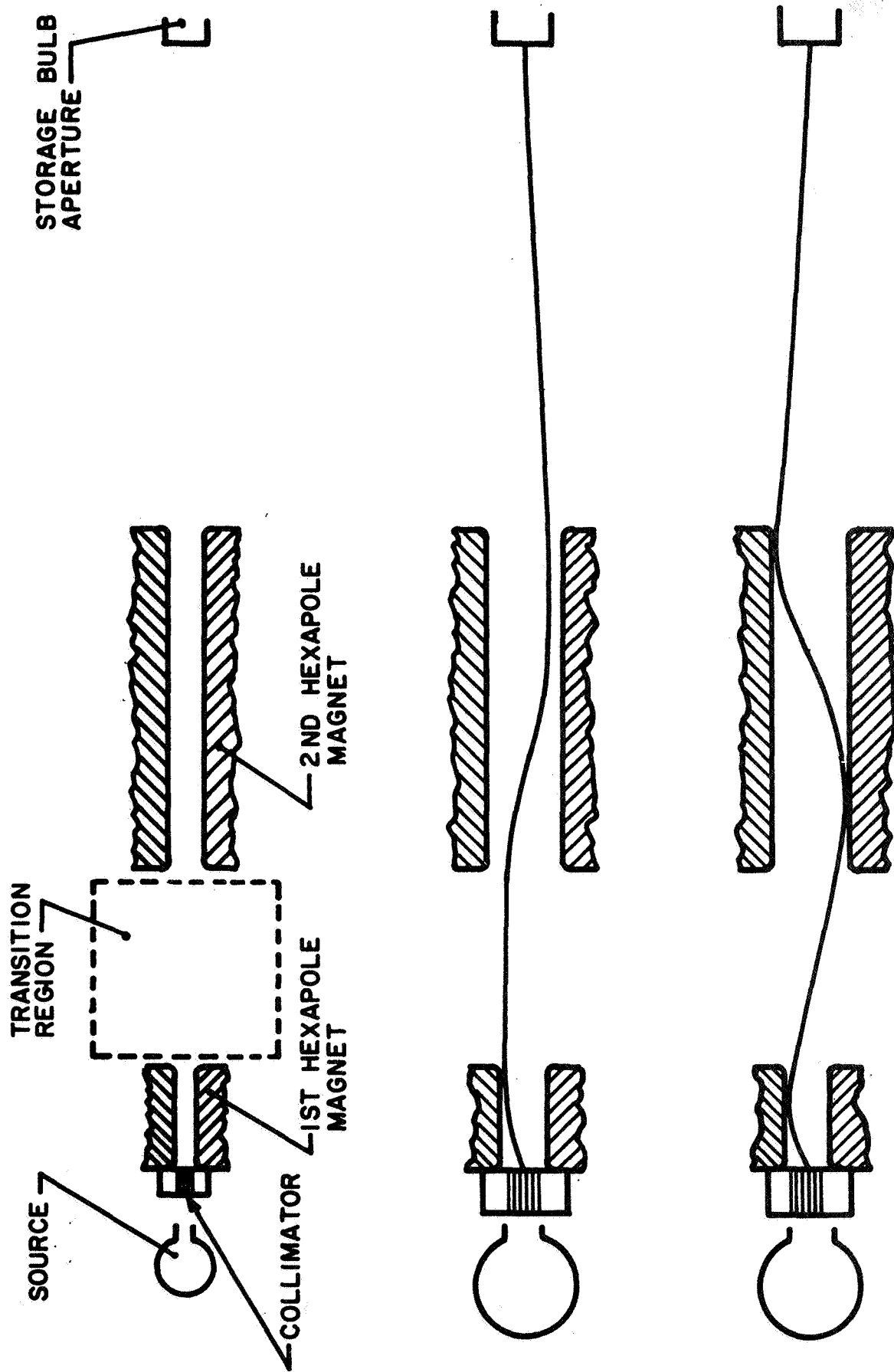
MAPSIN W/ RESTRICTION   1

STRAFO W/ LINEAR FORCE   2

STRAFO W/ BREIT-RABI   3

V/α

Figure 2B.

Figure 3.

TWO MAGNET SYSTEM

FIRST MAGNET TAPERED

MAPSIN 1

STRAFO 2

V/α

Figure 4.

$$I_{m=0} / I_{total} = (1 - 2\epsilon + 2\epsilon^2)/(1 + \epsilon^2)$$

$$\epsilon = 1 - T\frac{1}{2}, -\frac{1}{2}$$
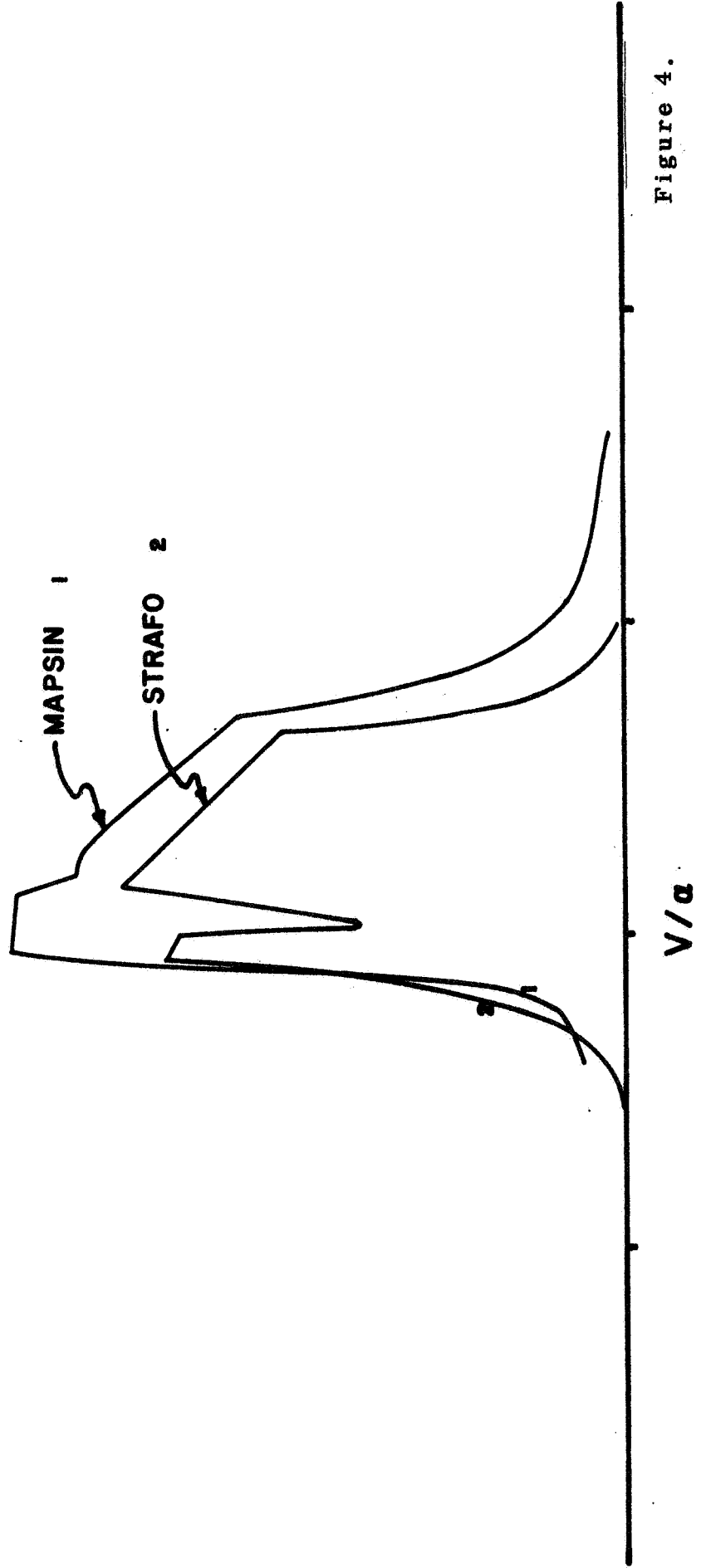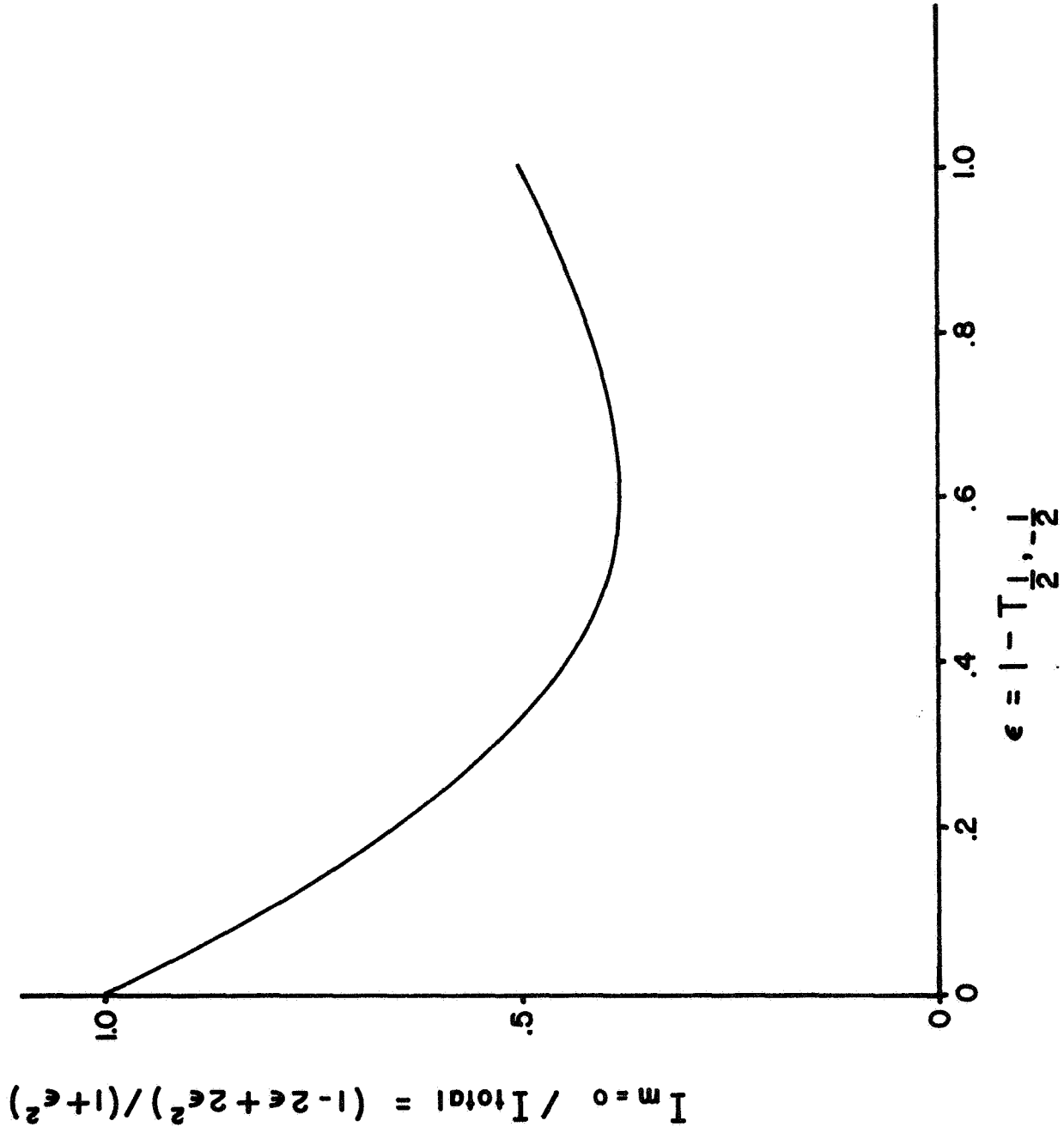
Figure 5.

Figure 6.

Figure 7.

A — RABI RESONANCE

B — ADIABATIC FAST PASSAGE

TIME OF FLIGHT

$T_{\frac{1}{2}, -\frac{1}{2}}$: SPIN 1/2 TRANSITION PROBABILITY
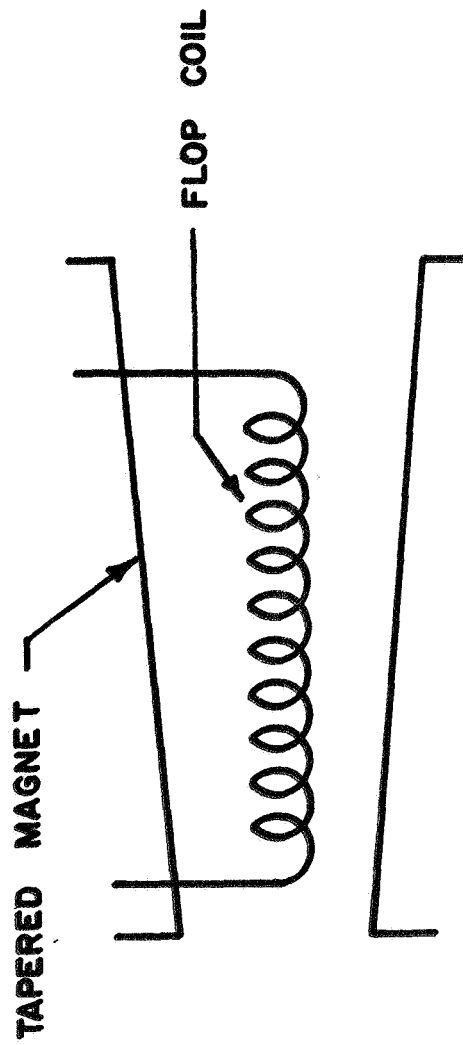
SHIELD

WINDING

FLOP COIL

A.

TAPERED MAGNET

FLOP COIL
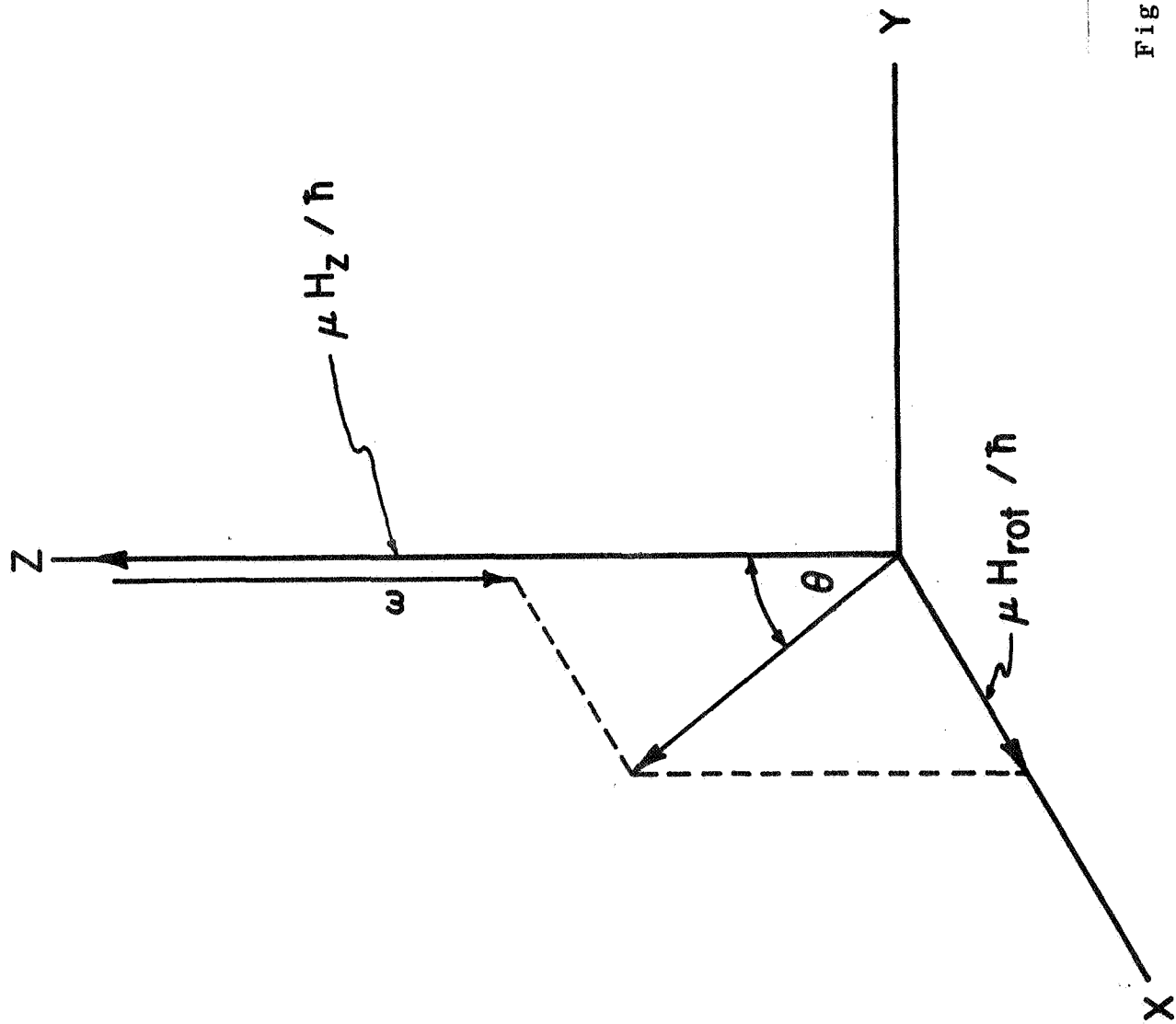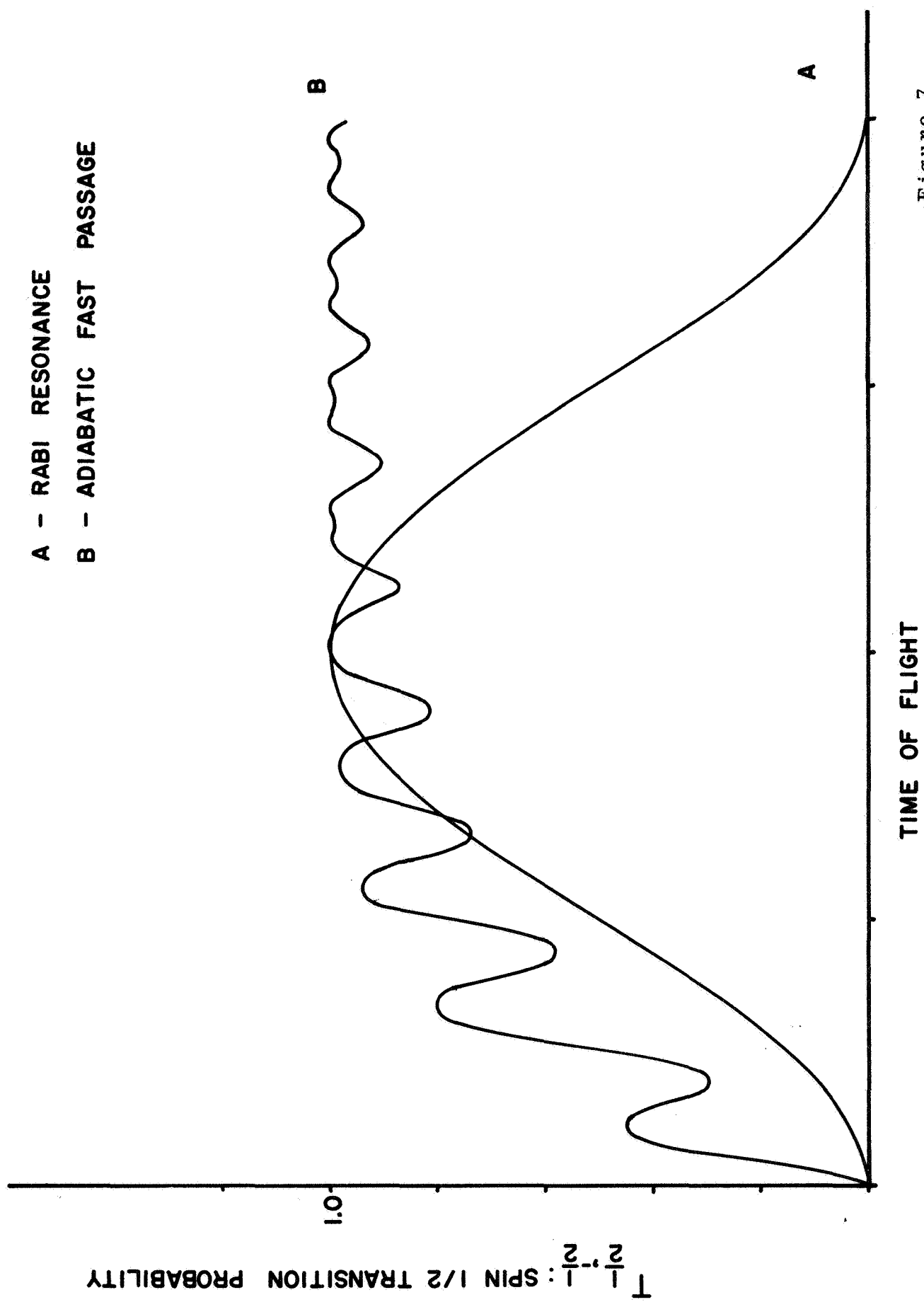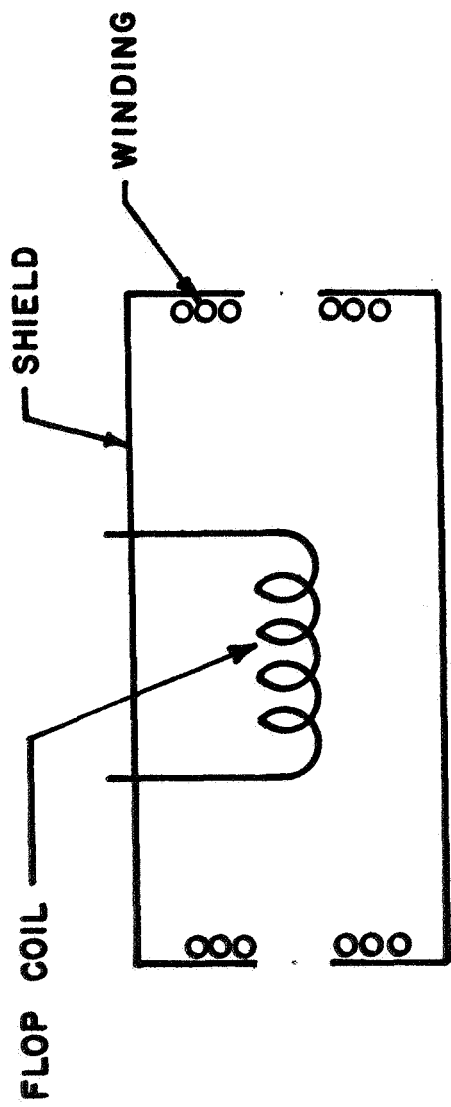
B.

ALTERNATIVE TRANSITION REGIONS

Figure 8.

STRAFO
LINEAR FORCE LAW

Figure 9.

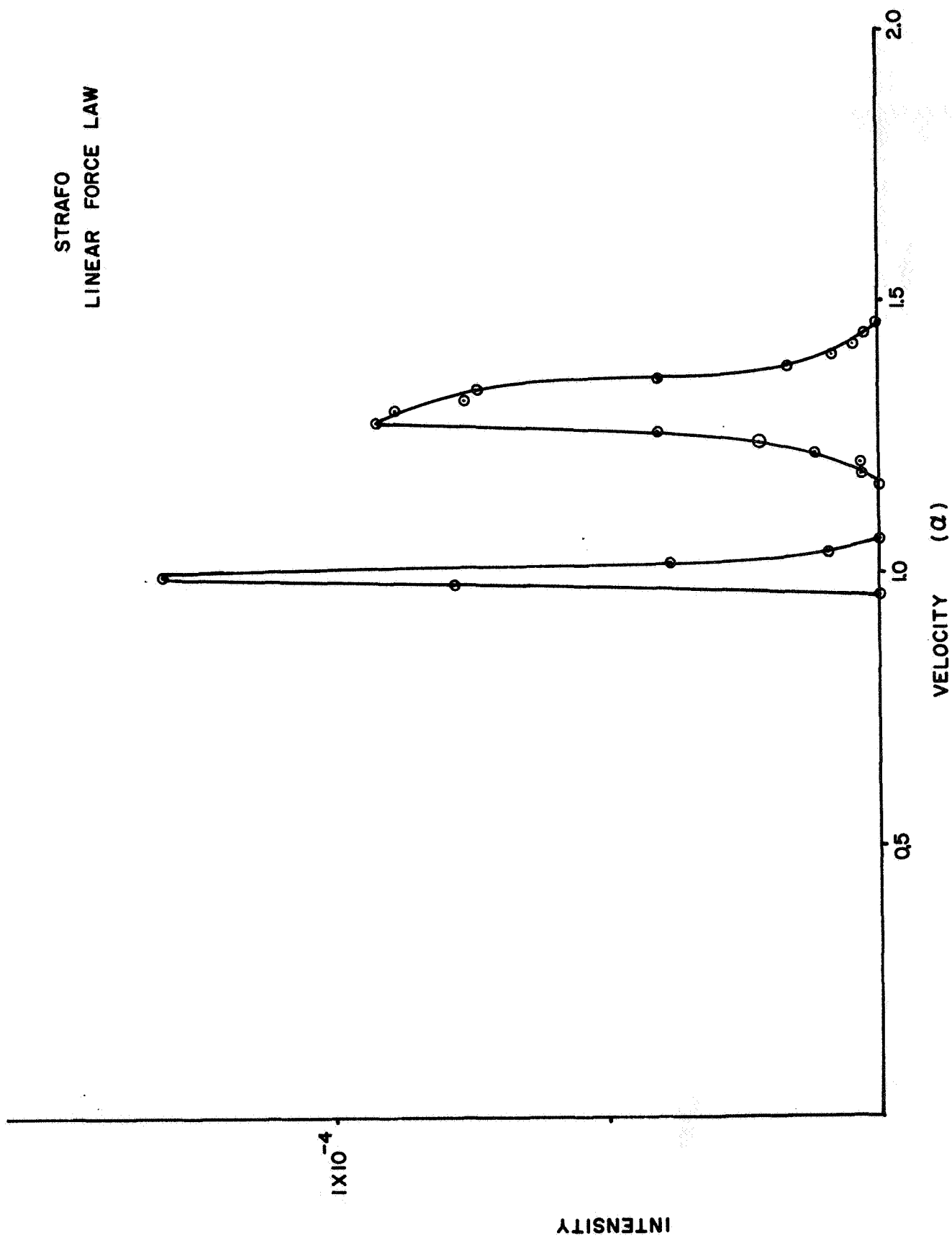STRAFO
BREIT - RABI FORCE LAW

VELOCITY (Ω)

INTENSITY
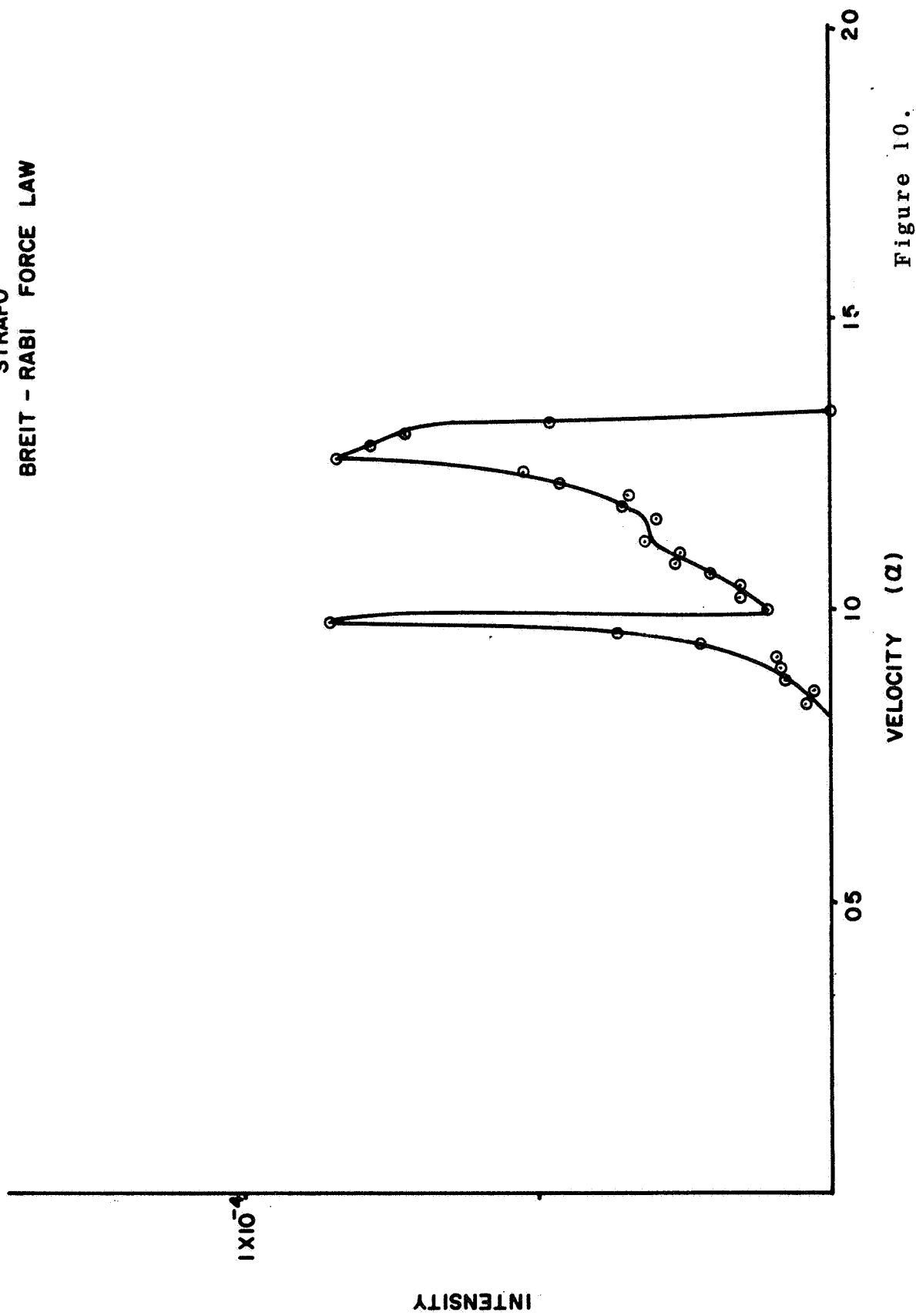
1×10⁻⁴

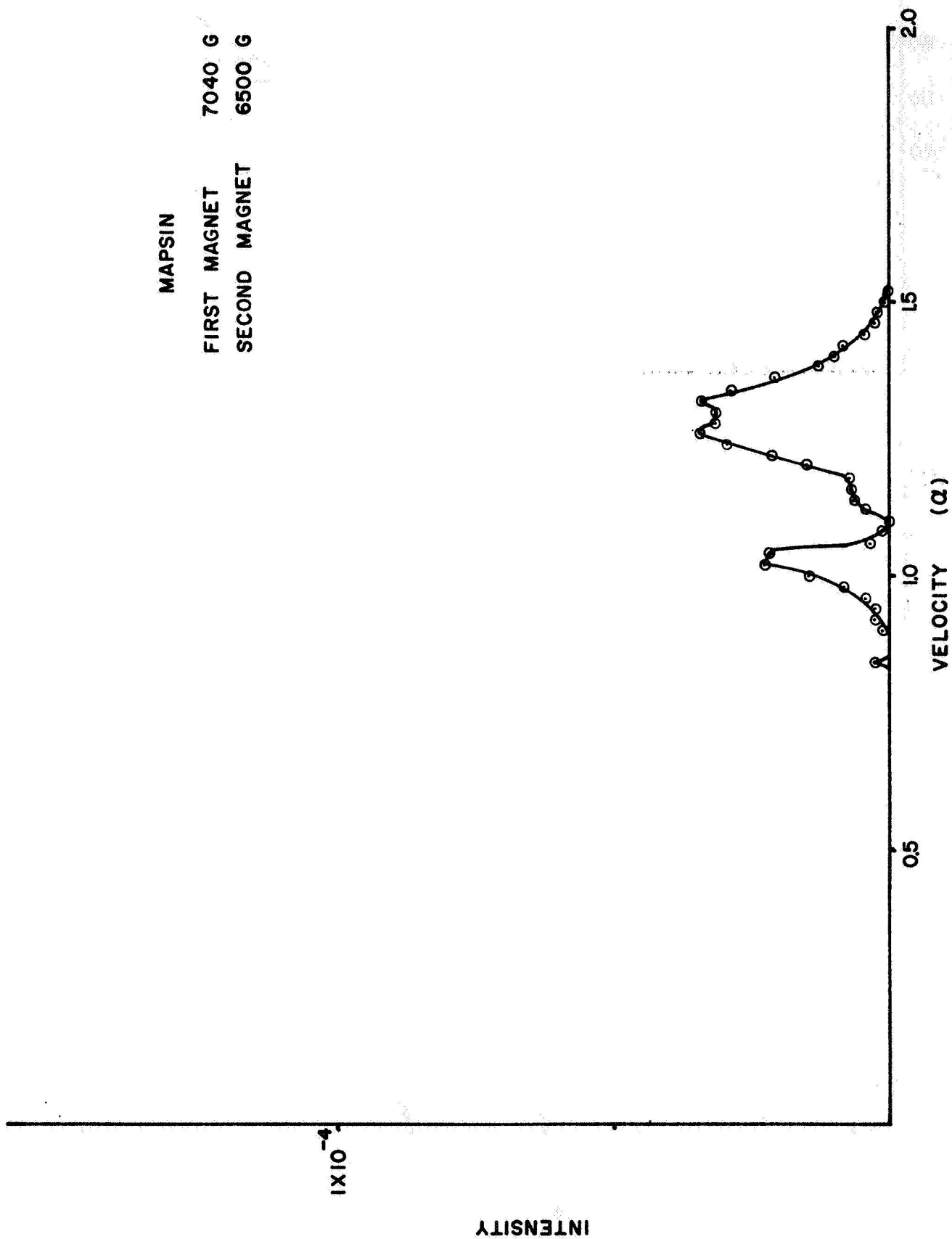05   10   15   20
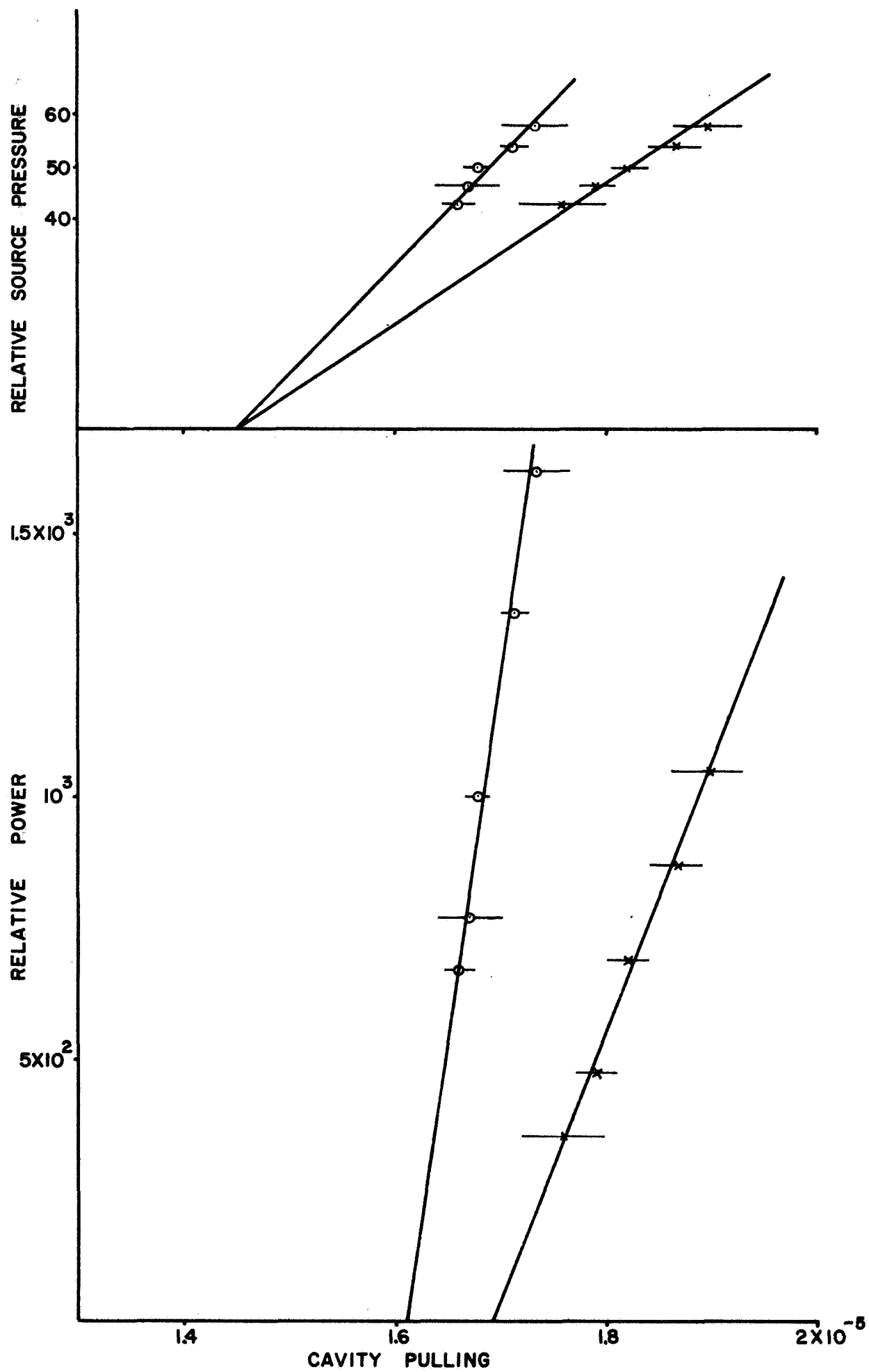
Figure 10.

Figure 11.

Figure 12.

<u>Appendix I</u>

Below is a listing of the program MAPSIN used to calculate the fraction of atoms effused from the collimator that reach the aperture of the storage bulb in a two magnet beam optics system for a hydrogen maser. We assume a Maxwell-Boltzmann velocity distribution at a temperature of 380 K. We provide the following data:

R1   the initial bore radius of the first magnet

T1   the taper of the first magnet

R2   the initial bore radius of the second magnet

T2   the taper of the second magnet

L1   the distance from the collimator to the first magnet

L2   the length of the first magnet

L3   the distance between magnets

L4   the length of the second magnet

L5   the distance from the second magnet to the target aperture

B$\emptyset$ the peak field strength in the magnets

M1 and M2 equal - 1 if the magnets deflect atoms away from axis

01   the exit radius of the first magnet

02   the radius of stop in exit plane of first magnet

03   the initial radius of the second magnet

04   the exit radius of the second magnet

05   the radius of stop in exit plane of second magnet

06   the radius of target aperture

07   the source radius

M3   the number of radial zones source is divided into

M5   the number of random initial slopes essayed from each zone

V1   the initial velocity in integrating over range of velocities

V2   the final velocity

V3   the velocity interval of each step

W2   the transmission factor of the collimator

The velocities are expressed as fractions of $\alpha\,(= \sqrt{2kT/m}\,)$

The magnetic field is in gauss

The linear dimensions must all be expressed in the same unit

```
...HPFTDE...

GE 600-LINE T/S FROM DARTMOUTH
TERMINAL 305 ON AT 11:28   10/30/68
USER NUMBER--V21581,HPFT
SYSTEM--BASIC
NEW OR OLD--OLD
OLD FILE NAME--MAPSIN
READY
LIST


MAPSIN          11:29          10/30/68


10 READ R1,T1,R2,T2,L1,L2,L3,L4,L5,B0
15 READ M1,M2
20 READ O1,O2,O3,O4,O5,O6,O7,M3,M5
25 READ V1,V2,V3,W2
40 LET K=SQR(1.7697E-7*B0)
50 FOR V=V1 TO V2 STEP V3
60 LET D=11
65 LET G=1
70 LET A=1
75 LET B=0
80 LET R=R1
85 LET L=L2
90 IF T1=0 THEN 140
100 LET T=T1
110 IF M1=-1 THEN 190
120 GOSUB 1000
130 GOTO 300
140 IF M1=-1 THEN 170
150 GOSUB 1100
160 GOTO 300
170 GOSUB 1200
180 GOTO 300
190 GOSUB 1300
300 LET D2=D6
305 LET D=D6
310 LET G2=G6
315 LET G=G6
320 LET A=A6
330 LET B=B6
340 LET D3=D+L3*A
345 LET D=D3
350 LET G3=G+L3*A
355 LET G=G3
360 LET L=L4
370 LET R=R2
```

```
380 IF T2=0 THEN 440
390 LET T=T2
400 IF M2=-1 THEN 490
410 GOSUB 1000
420 GOTO 600
440 IF M2=-1 THEN 470
450 GOSUB 1100
460 GOTO 600
470 GOSUB 1200
480 GOTO 600
490 GOSUB 1300
600 LET D4=D6
610 LET G4=G6
620 LET D5=D6+L.5*A6
630 LET G5=G6+L.5*B6
640 GOSUB 1400
650 NEXT V
660 PRINT "TOTAL FRACTIONAL INTENSITY=";O1
670 STOP
800 DATA .04,0,.0625,0,.125,2.112,4,7.0408,10,7500
810 DATA 1,1
820 DATA .04,0,.0625,.0625,0,.113,.005
830 DATA 5,100
840 DATA .7,2.3,.02,.1135
1000 LET H=SQR((K/(T*V))↑2-.25)
1010 LET P=H*LOG(1+T*L/K)
1020 LET C=SQR(1+T*L/K)
1030 LET C1=COS(P)
1040 LET S1=SIN(P)
1050 LET D6=C*(D*(C1-S1/(2*H))+A*K*S1/(T*H))
1060 LET G6=C*(G*(C1-S1/(2*H))+B*K*S1/(T*H))
1070 LET A6=(A*(C1+S1/(2*H))-D*T*(2*H+1/(2*H))*S1/(2*K))/C
1080 LET B6=(B*(C1+S1/(2*H))-G*T*(2*H+1/(2*H))*S1/(2*K))/C
1090 RETURN
1100 LET P=K*L/(V*R)
1110 LET D6=D*COS(P)+A*L*SIN(P)/P
1120 LET G6=G*COS(P)+B*L*SIN(P)/P
1130 LET A6=A*COS(P)-D*P*SIN(P)/L
1140 LET B6=B*COS(P)-G*P*SIN(P)/L
1150 RETURN
1200 LET P=K*L/(V*R)
1210 LET C=EXP(P)
1220 LET C1=(C+1/C)/2
1230 LET S1=(C-1/C)/2
1240 LET D6=D*C1+A*L*S1/P
1250 LET G6=G*C1+A*L*S1/P
1260 LET A6=A*C1+D*P*S1/L
1270 LET B6=B*C1+G*P*S1/L
1280 RETURN
```

```
1300 LET H=SQR((K/(T*V))↑2+.25)
1310 LET P=EXP(H*LOG(1+T*L/R))
1320 LET C=SQR(1+T*L/R)
1330 LET C1=(P+1/P)/2
1340 LET S1=(P-1/P)/2
1350 LET D6=C*(D*(C1-S1/(2*H))+A*R*S1/(T*H))
1360 LET G6=C*(G*(C1-S1/(2*H))+B*R*S1/(T*H))
1370 LET A6=(A*(C1+S1/(2*H))+D*T*(2*H-1/(2*H))*S1/(2*H))/C
1380 LET B6=(B*(C1+S1/(2*H))+G*T*(2*H-1/(2*H))*S1/(2*H))/C
1390 RETURN
1400 LET W1=2*V↑3*EXP(-V*V)*V3
1405 LET Q=0
1407 LET W=(O1/D2)↑2/W2
1410 FOR Y0=O7/(2*M3) TO O7*(1-1/(3*M3)) STEP O7/M3
1415 LET M=N=0
1420 IF (ABS(Y0*(G4/D4-G5/D5))+ABS(O6/D5))↑2<(O5/D4)↑2 THEN 1650
1430 IF (ABS(Y0*(G2/D2-G5/D5))+ABS(O6/D5))↑2<(O2/D2)↑2 THEN1650
1440 IF-Y0*G5/D5+ABS(O6/D5)<-Y0*G4/D4-ABS(O4/D4) THEN 1650
1450 IF-Y0*G5/D5-ABS(O6/D5)>-Y0*G4/D4+ABS(O4/D4) THEN 1650
1460 IF -Y0*G5/D5+ABS(O6/D5)<-Y0*G3/D3-ABS(O3/D3) THEN 1650
1470 IF -Y0*G5/D5-ABS(O6/D5)>-Y0*G3/D3+ABS(O3/D3) THEN1650
1480 IF -Y0*G5/D5+ABS(O6/D5)<-Y0*G2/D2-ABS(O1/D2) THEN1650
1490 IF -Y0*G5/D5-ABS(O6/D5)>-Y0*G2/D2+ABS(O1/D2) THEN 1650
1500 LET X=O1*RND/D2
1510 LET Y=2*O1*RND/D2-Y0*G2/D2-O1/D2
1530 IF (Y+Y0*G2/D2)↑2+X↑2>(O1/D2)↑2 THEN 1630
1535 IF Y↑2+X↑2>(K/V)↑2 +T1↑2 THEN 1600
1540 IF (Y+Y0*G2/D2)↑2+X↑2<(O2/D2)↑2 THEN 1600
1550 IF (Y+Y0*G3/D3)↑2+X↑2>(O3/D3)↑2 THEN 1600
1560 IF (Y+Y0*G4/D4)↑2+X↑2>(O4/D4)↑2 THEN 1600
1570 IF (Y+Y0*G4/D4)↑2+X↑2<(O5/D4)↑2 THEN 1600
1580 IF (Y+Y0*G5/D5)↑2+X↑2>(O6/D5)↑2 THEN 1600
1590 LET M=M+W
1600 LET N=N+1
1620 IF N>=M5 THEN 1640
1630 GOTO 1500
1640 LET Q=Q+W1*2*M*Y0/(N*M3*O7)
1650 NEXT Y0
1660 PRINT V,Q
1670 LET Q1=Q1+Q
1680 RETURN
9999 END


READY

BYE
OFF AT 11:35   10/30/68
```

Appendix II.

Below is a listing of the program STRAFO used to calculate the fraction of atoms effused from the collimator that reach the aperture of the storage bulb in a two-magnet beam optics system for a hydrogen maser. We assume a Maxwell-Boltzmann velocity distribution at a temperature of 380^0K. We provide the following data:

L1   the distance from collimator to first magnet
L2   the length of the first magnet
L3   the distance between magnets
L4   the length of the second magnet
L5   the distance from the second magnet to the target aperture

V1   the initial velocity in integrating over range of velocities
V2   the final velocity
V3   the velocity interval of each step

N1   the number of angular zones into which the cone of
       angle $(2\mu B_0/mV^2)^{1/2}$ is divided
N2   the number of steps through the first magnet
N3   the number of steps through the second magnet

R1   the radius of the first magnet
R2   the radius of the second magnet
R3   the radius of the storage bulb aperture

Bϕ the peak field strength in the magnets

W   the transmission factor of the collimator

The velocities are expressed in fractions of $\alpha \left[= (2kT/m)^{1/2} \right]$.

The magnetic field is expressed in gauss.

Linear dimensions must be expressed all in the same unit.

```
...HPFTDE...

GE 600-LINE T/S FROM DARTMOUTH
DISC STORAGE SHORTAGE. PLEASE UNSAVE UNNECESSARY PROGRAMS.
TERMINAL 311 ON AT 15:17   11/11/68
USER NUMBER--V21581,HPFT
SYSTEM--BASIC
NEW OR OLD--OLD
OLD FILE NAME--STRAFO
READY
LIST


STRAFO          15:18         11/11/68


10 READ L1,L2,L3,L4,L5
20 READ V1,V2,V3,N1,N2,N3
30 READ R1,R2,R3,B0,W
35 READ S1,S2
40 LET K=1.7721E-7*B0
50 LET K1=SQR(K)
60 LET Q1=0
70 FOR V=V1 TO V2 STEP V3
80 LET I=2*V3*V↑3*EXP(-V*V)
90 LET Q=0
100 LET D=K1/V
110 FOR M=1 TO N1
120 LET D1=(M-.5)*D/N1
130 LET D3=D1
140 LET R=D1*L1/R1
150 FOR J=1 TO N2
160 LET X=1.9758E-3*B0*R*R
170 LET A=-K*R*X/SQR(1+X*X)
180 LET D2=D1+A*L2/(R1*N2*V*V)
190 LET R=R+D1*L2/(R1*N2)+.5*A*(L2/(R1*N2*V))↑2
200 IF ABS(R)>=1 THEN 360
210 LET D1=D2
220 NEXT J
```

```
225 IF ABS(R)<S1/R1 THEN 350
230 LET R=(R1*R+L3*D1)/R2
240 FOR J=1 TO N3
250 LET X=1.9758E-3*B0*R*R
260 LET A=-K*R*X/SQR(1+X*X)
270 LET D2=D1+A*L4/(R2*N3*V*V)
280 LET R=R+D1*L4/(R2*N3)+.5*A*(L4/(R2*N3*V))↑2
290 IF ABS(R)>=1 THEN 350
300 LET D1=D2
310 NEXT J
315 IF ABS(R)<S2/R2 THEN 350
320 LET R=R*R2+L5*D1
330 IF ABS(R)>R3 THEN 350
340 LET Q=Q+2*I*D*D3/(N1*R)
350 NEXT M
360 PRINT V,Q
370 LET Q1=Q1+Q
380 NEXT V
390 PRINT "TOTAL FRACTIONAL INTENSITY=";Q1
800 DATA .125,2.112,4,7.0408,10
810 DATA .7,2.3,.02
820 DATA 10,10,30
830 DATA .04,.0625,.113
840 DATA 7500,.1135
850 DATA 0,0
999 END


READY

OLD
OLD FILE NAME--MAPSIN
READY
BYE
OFF AT 15:20  11/11/68
```

Appendix III

Below is a listing of the program ADIAFP used to calculate the transition probability for a spin $\frac{1}{2}$ particle in a rotating magnetic field as it passes through a static field that varies at a constant rate. We specify the following:

N   the number of zones the transition region is divided into

R   the range of the atomic resonance frequency in radians over the transition region divided by 2b

D   the strength of the rotating field: $D = bt$ (radians)

```
10 LET F1=1
20 LET F2=G1=G2=0
30 READ N,R
35 PRINT "NUMBER OF HALFWIDTHS AT START=";R/2
36 PRINT "NUMBER OF STEPS=";N
37 PRINT "TRANSITION","RADIANS"
38 PRINT "PROBABILITY","PRECESSED"
39 FOR D=15.5 TO 20 STEP .5
40 FOR M=1 TO N
45 LET Z=R*((M-.5)/N-.5)
50 LET Y1=1/SQR(1+Z↑2)
60 LET Y2=Y1*Z
70 LET X=D/(Y1*N)
80 LET C=COS(X)
90 LET S=SIN(X)
100 LET F3=F1*C-S*(Y2*F2-Y1*G2)
110 LET F4=F2*C+S*(Y2*F1-Y1*G1)
120 LET G3=G1*C+S*(Y1*F2+Y2*G2)
130 LET G4=G2*C-S*(Y1*F1+Y2*G1)
140 LET F1=F3
150 LET F2=F4
160 LET G1=G3
170 LET G2=G4
180 NEXT M
190 PRINT G1↑2+G2↑2,D
195 LET F1=1
196 LET F2=G1=G2=0
200 NEXT D
800 DATA 200,10
999 END
```